

UNCLASSIFIED



Australian Government

Department of Defence

Science and Technology

The Radiation Patterns of Circular Apertures

Dr J L Whitrow

**National Security and ISR Division
Defence Science and Technology Group**

DST-Group-TR-3487

ABSTRACT

Taylor, Bayliss, and Chesley are names associated with the design of antennas for modern pulse Doppler radar systems. This report provides a unified approach to the design techniques that they used to achieve the specified beam shape and sidelobe levels that are key performance requirements for airborne pulse-Doppler signal processing. A number of ancillary factors on signal and noise levels in the use of these antenna designs are discussed.

RELEASE LIMITATION

Approved for Public Release

UNCLASSIFIED

UNCLASSIFIED

Produced by

*National Security and ISR Division
PO Box 1500
Edinburgh, South Australia 5111, Australia*

Telephone: 1300 333 362

*© Commonwealth of Australia 2018
May, 2018*

AR-017-177

APPROVED FOR PUBLIC RELEASE

UNCLASSIFIED

The Radiation Patterns of Circular Apertures

Executive Summary

The design of low sidelobe phased array antennas is one of several key technical requirements in the development of the air-to-air modes of pulsed Doppler radar systems. A seminal work on controlling the sidelobes of such antennas was presented in a paper by Taylor [16]. He devised a technique to control the near-in sidelobes of an antenna by shifting the zeros of an appropriate realisable antenna pattern. Bayliss [3] subsequently used a similar technique to design the radiation pattern for monopulse position measurement as used for target tracking, and later Chesley [5] designed a delta-delta, or double difference, beam which is of benefit in the tracking of multiple targets and for some electronic protection techniques. Taylor weighting can be used for both transmission and reception, whereas Bayliss and Chesley designs are used only for reception of radar return signals.

The three aforementioned authors use different approaches in selecting the positions to which the zeros need to be shifted, but the surrounding mathematics is essentially the same. In this report a common mathematical structure is developed to treat all three design techniques. The basic idea is to start with an entire function of appropriate shape, (an entire function is a function expressible as a product of its zeros), and then determine how these zeros should be manipulated. To begin, a model antenna pattern is generated with the required sidelobe behaviour, but may not be physically realisable, and the positions of its zeros determined. The M^{th} zero of the model function is scaled to coincide with the M^{th} , (sometimes the $M + 1^{\text{th}}$) zero of the starting function, and the zeros up to the M^{th} of the starting function repositioned to the locations of the respective zeros of the scaled model function. The resulting antenna pattern then exhibits the required sidelobe behaviour for the first M sidelobes, has a minimum beamwidth commensurate with the sidelobe levels, and the far sidelobes taper off suitably at large angles.

The body of the work concludes with a discussion of gain, effective aperture and aperture efficiency, which are key parameters defining the quality of an antenna, and shows how they are deduced from the antenna designs. It is shown that these terms can be quite misleading when determining signal levels in receiving systems. Though there is only a slight loss in gain, of the order of 1 dB, between a uniform aperture and a Taylor weighted aperture, there can be as much as 7 dB reduction in received signal strength for the Taylor weighted aperture. Greater losses are incurred with the Bayliss and Chesley designs. The saving feature in the use of these designs is that there is a similar reduction in the received noise so that the overall loss in signal-to-noise ratio is relatively small.

UNCLASSIFIED

This page is intentionally blank

UNCLASSIFIED

Author



John L Whitrow

Daintree Systems

John Whitrow joined the then WRE as a Cadet, Defence Science in 1963, while studying for a combined science and electrical engineering degree at the University of Adelaide. Upon graduation, he was appointed as a Scientific Officer in Electronic Techniques Group where he worked on electromagnetic theory, antennas and microwave components. Between 1971 and 1974 he carried out research for a Ph.D. in electromagnetic diffraction theory at Monash University, continuing in the same line of research on return to Edinburgh. In 1979 he was promoted to SRS to work on the analysis of microwave radar system performance. In this period, he also represented the Department of Defence in the development of Australian Standard AS-2772 covering exposure of personnel to microwave radiation. In 1990 he became a Group Head, continuing to work on microwave radar systems. During his career, he has been involved in providing radar system advice on a number of major acquisition projects. His primary interest has been the analysis of performance of airborne pulse Doppler radar systems, for both air-to-air and air-to-sea-surface applications. He retired in November 2007, but since March 2009 has been employed as a contractor through Daintree Systems to provide support on radar matters for the acquisition of the F-35 Lightning aircraft. He has authored several reports on the characteristics and performance of the APG-81 radar in the F-35.

UNCLASSIFIED

This page is intentionally blank

UNCLASSIFIED

Contents

1	INTRODUCTION	1
2	BASIC ANTENNA PROPERTIES	2
3	RADIATION BY A CIRCULAR APERTURE	4
	3.1 Uniform Aperture Distribution	6
	3.2 Taylor Aperture Distribution	8
	3.3 Bayliss Aperture Distribution	15
	3.4 Delta-Delta Aperture Distribution	24
4	DIRECTIVITY, APERTURE EFFICIENCY, AND NOISE PROPERTIES OF APERTURE DISTRIBUTIONS	31
5	CONCLUSIONS	37
	REFERENCES	38
	APPENDIX A: IMPLEMENTATION OF THE ALGORITHMS IN MATHE- MATICA	41
	A.1 The Setup Procedure	41
	A.2 Calculation of the Antenna Fields	43

UNCLASSIFIED

This page is intentionally blank

UNCLASSIFIED

1. Introduction

The first effective airborne pulse Doppler radar systems used slotted waveguide antennas divided into four sectors for reception of target returns, the sum of the sectors providing what is called the sum beam, the difference between the sum of the top two and the bottom two sectors providing the elevation difference beam, and the difference between the left two and the right two sectors the azimuth difference beam. There is a fourth beam, formed by the assembly of hybrid T junctions used to form the sum and difference beams, that originally was terminated in a dummy load. In more recent radar systems, this beam, called the double difference or delta-delta beam, has been used to resolve monopulse measurements of two targets within the main beam, and to implement certain electronic protection techniques. The performance of these radars in detecting targets using medium pulse repetition frequency waveforms depended critically on the sidelobe performance of the sum beam, but the way the beams were produced required compromises in the radiation patterns, particularly the sidelobe levels of the difference beams. The basic technique for designing low-sidelobe sum beams was published by Taylor [16] in 1960, and in 1967 Bayliss [3] reported his technique for designing monopulse antenna beams. Much later, in 1992, Chesley [5] published a technique for the design of what he called the double difference beam shape. General techniques for designing circular aperture antennas were published by Ruze [15] in 1964. However, it is only with the advent of modern electronically scanned phased array radars, that these techniques may be exploited to full advantage. Such radars may have several thousand transmit/receive modules, the receive outputs of which are combined in a set of manifolds, each of which can be optimised for the individual beams introduced above. Hence our interest in the above antenna design techniques as they are critical to modern radar performance. Because of the importance of these designs to pulse-Doppler radar system performance, the radiation patterns of circular uniformly distributed apertures and Taylor distributed apertures are commonly discussed in advanced radar texts, [14], as well as most antenna texts, [7]. In this report we examine all these techniques in a common mathematical structure, and investigate some issues not normally discussed in texts on pulse-Doppler radar systems, but which are important in the radar system performance studies we wish to undertake.

Although our interest is in the properties of phased array antennas, we will initially focus on the radiation patterns of circular antennas with specific field distributions across the aperture. Our assumption is that phased arrays with a thousand or more elements, whose element distributions closely follow the aperture distribution, can be satisfactorily represented by the above designs. Elliott [8] discusses the effects of the discretisation of the continuous aperture distribution to assess phased array performance, but we do not consider this issue here. When we look at the noise properties of phased array antennas, we will have the need to consider the elements of the array.

The basic idea of all three radiation pattern designs is to start with a suitable realisable antenna pattern which is an entire function [4] of the scan angle¹. A model function is then sought which has the desired sidelobe behaviour, but may not be a realisable antenna radiation pattern. The position of the zeros of this function are then determined, and used to adjust the positions of a few of the inner zeros of the starting function. The net result is a realisable

¹An entire function is a function which is expressible as a product of its zeros

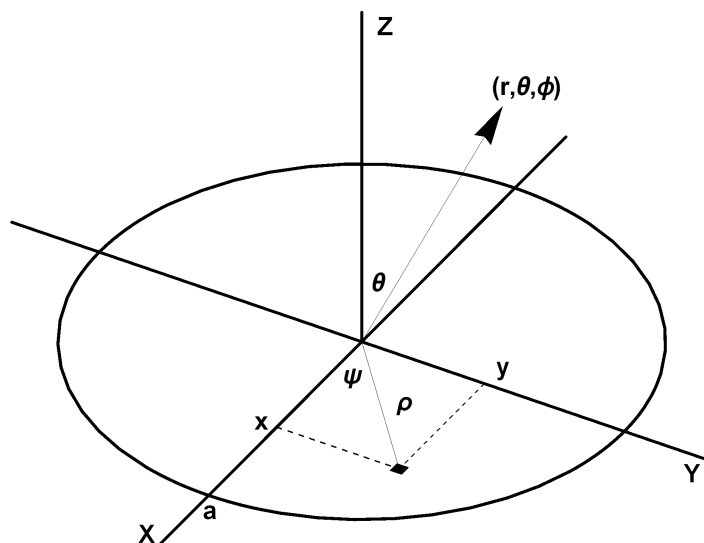


Figure 1: Coordinate systems for the circular antenna of radius a

antenna radiation pattern in which the inner sidelobe levels are close to those of the model function, and the outer sidelobes taper off at a suitable rate so that there are no problems in implementation of the radiation pattern.

Having discussed these techniques as applied to the sum, difference and double difference beams, we look at other properties of the antenna designs which need to be considered in the development of models of pulse Doppler radar systems. In multielement phased arrays, the concept of gain is not well defined. The gain of a Taylor weighted phased array is not much less than that of a uniform array, but because the power across the aperture is tapered, less total power is transmitted, and thus there is a considerable reduction in radiated signal strength. A similar effect is observed in reception performance. We do not claim any originality for these results; every radar house will need to do these calculations in the design of their radar systems. It is just that these results are not widely published and so needed to be generated for a current study which makes it worthwhile recording them for future studies.

2. Basic Antenna Properties

In this work, we shall replace the phased array antenna with an aperture, the radiation properties of which can be determined from the electric field distribution in the aperture. We start with a circular aperture of radius a , and, without loss of generality, specify that the electric field in the aperture is directed parallel to the X axis, and has the form locally of a plane wave propagating orthogonal to the aperture. The radiated field is to be calculated at the point (r, θ, ϕ) , in standard spherical polar coordinates, in the far field of the aperture. The electric field in the aperture is $E_a(x, y)$, where x and y are the coordinates of the field point. This point is also described by the cylindrical polar coordinates (ρ, ψ) . The relationship of these coordinates is illustrated in Figure 1. A time harmonic dependency of the fields of the form $e^{j\omega t}$ is assumed, with an associated wavelength λ of the radiation and wave number $k = 2\pi/\lambda$.

The components of the electric field strength at (r, θ, ϕ) [2], [14] are, in the $\hat{\theta}$ direction,²

$$E_{\theta}(r, \theta, \phi) = \frac{jkAe^{-jkr}}{2\pi r} \frac{1 + \cos \theta}{2} \cos \phi F(\theta, \phi) \quad (1)$$

and, in the $\hat{\phi}$ direction,

$$E_{\phi}(r, \theta, \phi) = \frac{jkAe^{-jkr}}{2\pi r} \frac{1 + \cos \theta}{2} \sin \phi F(\theta, \phi) \quad (2)$$

where $A = \pi a^2$ is the area of the aperture, and

$$F(\theta, \phi) = \frac{1}{\pi a^2} \iint_A E_a(x, y) e^{jk(x \sin \theta \cos \phi + y \sin \theta \sin \phi)} dx dy \quad (3)$$

The field strength in the direction of \hat{r} is negligibly small in the far field. Since the directions $\hat{\theta}$ and $\hat{\phi}$ are orthogonal, and the components of the field in these directions are proportional respectively to $\cos \phi$ and $\sin \phi$, it follows that the amplitude E of the electric field strength is

$$E(r, \theta, \phi) = \frac{jkAe^{-jkr}}{2\pi r} \frac{1 + \cos \theta}{2} F(\theta, \phi) \quad (4)$$

The reason for the normalisation term in the expression for $F(\theta, \phi)$, the area of the aperture, πa^2 , which other authors do not use, is that it will simplify the expressions that are developed later.

It is possible to directly carry out the integrations of equation 3 with respect to x and y , but it is preferable to replace these coordinates of the aperture with the cylindrical coordinates $\{\rho, \psi\}$ shown in figure 1, thus

$$x = \rho \cos \psi \quad (5)$$

$$y = \rho \sin \psi \quad (6)$$

$$dx dy = \rho d\rho d\psi \quad (7)$$

simplifying equation 3 to

$$F(\theta, \phi) = \frac{1}{\pi a^2} \int_0^{2\pi} \int_0^a E_a(\rho, \psi) e^{jk\rho \sin \theta \cos(\phi - \psi)} \rho d\rho d\psi \quad (8)$$

In the far field of the antenna, the electric and magnetic field vectors are orthogonal and related by the characteristic impedance of free space, Z_0 . The average radiated power per unit solid angle in the direction $\{\theta, \phi\}$ is

$$P(\theta, \phi) = \frac{1}{2Z_0} r^2 |E(r, \theta, \phi)|^2 \quad (9)$$

The factor $1/2$ arises from the fact that the electric field varies in amplitude as $\exp(j\omega t)$. In some antenna texts, the term $(1 + \cos \theta)^2/4$ in the expression for the radiated power is referred

²The symbol $\hat{\cdot}$ above a coordinate parameter indicates a unit vector in the direction that the coordinate increases.

to as the obliquity factor and $|F(\theta, \phi)|^2$ as the space factor; we shall use this terminology for both the factors in equation 4 and their squares, the context providing the appropriate meaning.

To calculate the total power transmitted by the aperture, we assume that at the aperture surface, the radiated field is a plane wave directed orthogonal to the aperture, and hence we can integrate over the aperture.

$$P_t = \frac{1}{2Z_0} \int_0^{2\pi} \int_0^a |E_a(\rho, \psi)|^2 \rho d\rho d\psi \quad (10)$$

The directivity³ of an antenna is defined as the ratio of the peak radiated power per unit solid angle to the average radiated power per unit solid angle, and is equal to $4\pi P(\theta, \phi)/P_t$. Aperture efficiency is a related parameter, used to assess the relative performance of apertures, and is defined as the directivity of the aperture divided by the directivity of a uniformly distributed aperture of the same size. With $E_a(\rho, \psi)$ constant in equations 9 and 10, for a uniform aperture, the peak directivity in the direction $\theta = 0^\circ$ normal to the aperture, is

$$D = \frac{4\pi^2 a^2}{\lambda^2} \quad (11)$$

3. Radiation by a Circular Aperture

We now wish to develop the mathematics that is common to all three antenna pattern designs. It is convenient to introduce two new variables, $u = 2a \sin \theta / \lambda$, and $p = \pi \rho / a$, into equation 8, simplifying its form to

$$F(\theta, \phi) = \frac{1}{\pi^3} \int_0^\pi \int_0^{2\pi} p E_a(p, \psi) e^{j u p \cos(\phi - \psi)} d\psi dp \quad (12)$$

The aperture distribution can be expanded as a combination of Bessel functions of the first kind in p , and a Fourier series in ψ ,

$$E_a(p, \psi) = \sum_{n=-\infty}^{\infty} \sum_{l=0}^{\infty} B_{n,l} e^{j n \psi} J_n(\mu_{n,l} p) \quad (13)$$

The Bessel functions exhibit orthogonality properties that, with appropriately chosen $\mu_{n,l}$, simplify the determination of the $B_{n,l}$. The value of n is constrained to the integers because the field is periodic in 2π . In fact, we will only need a finite number of terms in n to describe the beam shapes discussed in this report. The simplest form is $n = 0$, a single term, for the generation of the Taylor radiation patterns, whereas $n = \pm 1$ for the Bayliss patterns, and $n = \pm 2$ for the delta-delta patterns. Thus the expansion of $E_a(p, \psi)$ reduces to

$$E_a(p, \psi) = \sum_n \sum_{l=0}^{\infty} B_{n,l} e^{j n \psi} J_n(\mu_{n,l} p) \quad \text{where} \quad \begin{cases} n = 0, & \text{Taylor} \\ n = \pm 1, & \text{Bayliss} \\ n = \pm 2, & \text{delta delta} \end{cases} \quad (14)$$

³The term gain, which is commonly used in describing antennas, includes both the effect of the beamshape, and ohmic and mismatch losses within the antenna; directivity depends only on the beamshape.

Noting that $J_{-n}(z) = (-1)^n J_n(z)$, [1], the summation over n for all the designs ultimately becomes a single term containing the product of a trigonometric function and a series of Bessel functions of the first kind of order n .

To simplify equation 12, use is made of the generating function for Bessel functions, ([9] equation 8.511.4)

$$e^{jz \cos \phi} = \sum_{m=-\infty}^{\infty} j^m J_m(z) e^{jm\phi} \quad (15)$$

which on replacing z with up , and ϕ with $\phi - \psi$ and substituting the result into equation 12 provides

$$F(\theta, \phi) = \frac{1}{\pi^3} \sum_{l=0}^{\infty} \sum_{m=-\infty}^{\infty} \sum_n j^m e^{jm\phi} B_{n,l} \int_0^\pi \int_0^{2\pi} p J_n(\mu_{n,l} p) J_m(up) e^{j(n-m)\psi} d\psi dp \quad (16)$$

The integral with respect to ψ is zero for $m \neq n$, and has the value 2π when $m = n$. Thus we find that

$$F(\theta, \phi) = \frac{2}{\pi^2} \sum_{l=0}^{\infty} \sum_n j^n e^{jn\phi} B_{n,l} \int_0^\pi p J_n(\mu_{n,l} p) J_n(up) dp \quad (17)$$

We now need to choose the $\mu_{n,l}$ to provide an appropriate solution for the aperture function. Guidance on the appropriate choice can be gained by observing that [18]

$$\begin{aligned} \int_0^\pi p J_n(\mu p) J_n(up) dp &= \frac{\pi u J_{n-1}(\pi u) J_n(\pi \mu) - \pi \mu J_{n-1}(\pi \mu) J_n(\pi u)}{\mu^2 - u^2} \\ &= \frac{\pi u J_n(\pi \mu) J_n'(\pi u) - \pi \mu J_n(\pi u) J_n'(\pi \mu)}{\mu^2 - u^2} \end{aligned} \quad (18)$$

where in the second line we have made use of the recursion relationship for the derivative of the Bessel functions ([1] equation 9.1.27)

$$J_n'(z) = J_{n-1}(z) - \frac{n J_n(z)}{z} \quad (19)$$

to replace the term in J_{n-1} by terms in J_n and its derivative⁴. There are two main options for selecting the values of μ ; we can either choose μ such that $J_n(\pi \mu) = 0$, in which case the first term of equation 18 is identically zero, or such that $J_n'(\pi \mu) = 0$, resulting in the second term being identically zero. Since the surface field distribution is expanded as a sum of terms of the form $J_n(\mu p)$, on the boundary of the antenna aperture, on which $p = \pi$, the first case forces the field to be zero, which has implications for aperture efficiency for a given sidelobe level. Hence there is a preference to define μ as the zeros of $J_n'(\pi \mu)$ as this choice provides a non-zero field at the edge of the aperture.

Thus, with $J_n'(\pi \mu) = 0$,

$$\int_0^\pi p J_n(\mu p) J_n(up) dp = \frac{\pi u J_n(\pi \mu) J_n'(\pi u)}{\mu^2 - u^2} \quad (20)$$

⁴In the notation $J_n'(\pi u)$ used in equation 18, and elsewhere in this report, we mean $dJ_n(x)/dx|_{x=\pi u}$.

and

$$F(\theta, \phi) = \frac{2}{\pi^2} \sum_{l=0}^{\infty} \sum_n j^n e^{jn\phi} B_{n,l} \frac{\pi u J_n(\pi \mu_{n,l}) J_n'(\pi u)}{\mu_{n,l}^2 - u^2} \quad (21)$$

Figure 2 shows the Bessel function derivatives of interest in this report, $J_0'(\pi u)$, $J_1'(\pi u)$, and $J_2'(\pi u)$ for u from 0 to 10. Note that both $J_0'(\pi u)$ and $J_2'(\pi u)$ have zeros at $u = 0$, whereas $J_1'(\pi u)$ has the value 0.5. Also, the zeros of $J_0'(\pi u)$ and $J_2'(\pi u)$ become closer to each other as u increases.

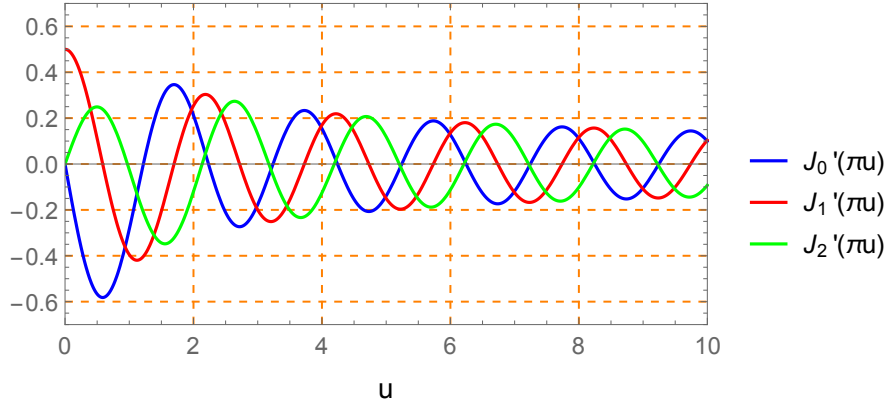


Figure 2: Derivatives of Bessel functions of the first kind, orders 0, 1, and 2

For large μ and fixed n , the $J_n'(\pi\mu)$ are asymptotic to (see [1] equation 9.2.1)

$$J_n'(\pi\mu) = -\sqrt{\frac{2}{\pi^2\mu}} \sin \pi \left(\mu - \frac{n}{2} - \frac{1}{4} \right) \quad (22)$$

and thus their zeros are approximated by

$$\mu_{n,l} = l + \frac{n}{2} + \frac{1}{4}, \quad l = 0, 1, 2 \dots \quad (23)$$

and provide a convenient starting point for the FindRoot function of *Mathematica*. Table 1 lists the first twenty zeros of these functions. Note that the zeros of $J_0'(\pi u)$ and $J_2'(\pi u)$ at the origin of figure 2 are not included in the table.

3.1. Uniform Aperture Distribution

We begin the discussion of specific aperture distributions with the uniform aperture distribution, which provides a reference point for discussing the gain and aperture efficiencies of the following designs. The calculation of $F(\theta, \phi)$ is straightforward as E_a is equal to 1, and $F(\theta, \phi)^5$ is independent of ϕ . Thus, instead of using equation 21, we begin with a simpler

⁵Throughout the text we refer to both $F(\theta, \phi)$ and $F(u)$, on the understanding that the F's are different but closely related; $F(u)$ contains all the terms of $F(\theta, \phi)$ that do not have an explicit dependence on ϕ , and thus both functions achieve the same peak value. Only in the case of the uniform and Taylor weightings are the functions identical, such as in equation 24, since these patterns are independent of ϕ .

Table 1: The first twenty zeros of $J_0'(\pi z)$, $J_1'(\pi z)$, and $J_2'(\pi z)$

l	$\mu_{0,l}$	$\mu_{1,l}$	$\mu_{2,l}$	l	$\mu_{0,l}$	$\mu_{1,l}$	$\mu_{2,l}$
1	1.21967	0.58607	0.97219	11	11.2466	10.7417	11.2286
2	2.23313	1.69705	2.13463	12	12.2469	11.7424	12.2303
3	3.23832	2.71719	3.17338	13	13.2471	12.7430	13.2318
4	4.24106	3.72614	4.19226	14	14.2473	13.7435	14.2331
5	5.24276	4.73123	5.20358	15	15.2475	14.7440	15.2342
6	6.24392	5.73452	6.21115	16	16.2477	15.7444	16.2352
7	7.24476	6.73683	7.21659	17	17.2478	16.7447	17.2360
8	8.24539	7.73854	8.22068	18	18.2479	17.7450	18.2368
9	9.24589	8.73985	9.22388	19	19.2480	18.7453	19.2375
10	10.2463	9.74089	10.2264	20	20.2481	19.7455	20.2381

version of equation 12, and it is developed as shown.

$$\begin{aligned}
F(\theta, \phi) = F(u) &= \frac{1}{\pi^3} \int_0^\pi \int_0^{2\pi} p e^{j u p \cos \psi} d\psi dp \\
&= \frac{1}{\pi^3} \sum_{m=-\infty}^{\infty} \int_0^\pi \int_0^{2\pi} j^m p J_m(up) e^{j m \psi} d\psi dp \\
&= \frac{2}{\pi^2} \int_0^\pi p J_0(up) dp \\
&= \frac{2 J_1(\pi u)}{\pi u} \\
&= -\frac{2 J_0'(\pi u)}{\pi u}
\end{aligned} \tag{24}$$

The second line uses the Bessel function expansion of the exponential function introduced in equation 15, the third line follows since the integral with respect to ψ is zero for all m not equal to zero, and equal to 2π for m equal to zero, the fourth line can be verified with [18], and the final line follows from [1], equation 9.1.28. At this stage we see the purpose of the normalisation introduced in the previous section; the peak value of $F(u)$, at $u = 0$, is unity, for a unit aperture field strength, and provides a convenient reference for assessing the three distributions of the following sections.

The function developed in equation 24 is an entire function (of the complex plane), which is expressible as a product of its zeros [4], multiplied by a constant to give it the correct value at $u = 0$; in this case the constant is unity. Figure 3 compares the functions $J_0'(\pi u)$ and $2J_0'(\pi u)/\pi u$; in particular it shows that with the second function the term πu in the denominator removes the zero of $J_0'(\pi u)$ at the origin, but the position of all the other zeros remain identical, and are symmetrically placed around the origin. Thus we can write

$$\begin{aligned}
F(u) &= \prod_{\substack{l=-\infty \\ l \neq 0}}^{\infty} 1 - \frac{u}{\mu_{0,l}} \\
&= \prod_{l=1}^{\infty} 1 - \left(\frac{u}{\mu_{0,l}} \right)^2
\end{aligned} \tag{25}$$

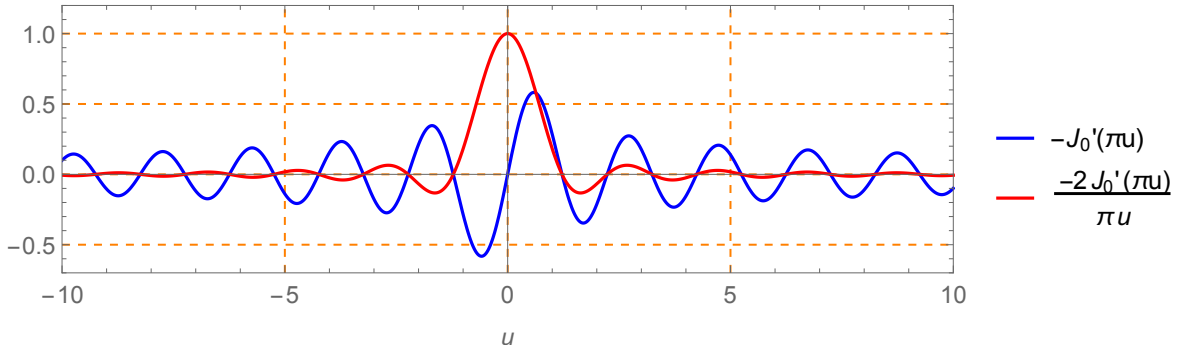


Figure 3: Comparison of the functions $J_0'(\pi u)$ and $2J_0'(\pi u)/\pi u$

where $\mu_{0,l}$ is the l^{th} zero of $J_0'(\pi u)$.

Figure 4 shows the space factor $F(u)$, where $u = 2a \sin \theta/\lambda$, of the radiation pattern of a 10 wavelength radius uniform aperture on a decibel scale, for angles in the range 0 to 90 degrees. The sidelobes gradually decay with angle to about -50 dB, but the first sidelobe at -17.6 dB is higher than desired for pulse-Doppler radar applications. Given that the radiation pattern is described by an entire function, the sidelobes can be manipulated by changing the positions of some of the zeros of the function, without affecting the peak amplitude of the radiation pattern since this occurs at the origin. However, the field in the aperture will need to increase in part, and reduce elsewhere, to maintain the peak radiated field strength at unit amplitude, and that raises questions of what we mean by the gain of such an array. The other point of interest in the radiation pattern is the gradual stretching of the interval between adjacent nulls when the pattern is plotted in θ space, whereas in u space the intervals are of uniform width. This property of u space is exploited in determining where to position the antenna beams of a phased array to cover the requested surveillance volume, but this is a topic for a separate report.

And that brings us to a discussion of Taylor weighting.

3.2. Taylor Aperture Distribution

In 1960, Taylor [16] published a technique for designing a circular aperture, the radiation pattern of which is a pencil beam uniform in azimuth, of minimum beamwidth commensurate with the near-in sidelobes satisfying a design level requirement, and the far sidelobes decaying at the same rate as a uniform aperture distribution. In the same journal, Hansen [10] published tables of the Taylor distributions for ease of application of Taylor's technique. The technique that Taylor developed was to pick a model function with the desired sidelobe structure, determine the positions of its zeros, and then modify some of the near-in zeros of a realisable antenna function to coincide with the same number of model function zeros.

Although we have a big hint from the previous section of where to start with the development of the radiation pattern, for the sake of consistency with the later antenna designs, let us return to the expansion in equation 17 of the field $F(\theta, \phi)$ in terms of the Bessel functions that describe the aperture distribution. Firstly, to have a pencil beam uniform in ϕ , the value

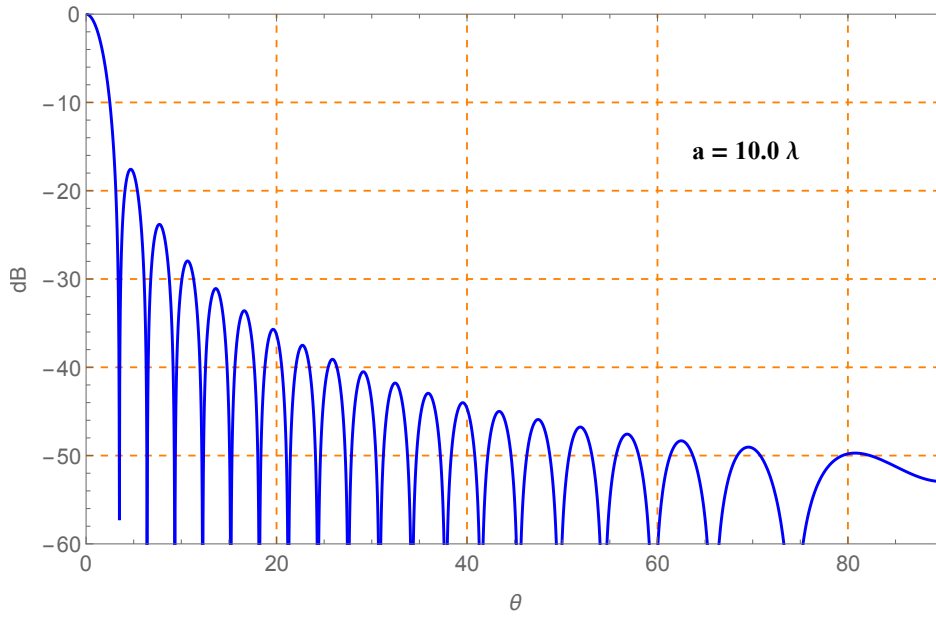


Figure 4: Radiation pattern of a 10 wavelength radius uniform distributed aperture

of n must be restricted to 0. The most significant term of the resulting expansion is provided by the zero of $J_0(\pi\mu)$ at the origin, and since $J_0(0) = 1$, this term becomes

$$\begin{aligned} \frac{2}{\pi^2} B_{0,0} \int_0^\pi p J_0(up) dp &= 2 B_{0,0} \frac{J_1(\pi u)}{\pi u} \\ &= -2 B_{0,0} \frac{J_0'(\pi u)}{\pi u} \end{aligned} \quad (26)$$

Apart from the constant $B_{0,0}$, this is the result for the radiated field of the uniform aperture. The expansion of the integral is verifiable with [18]. Thus a suitable starting function is

$$F_S(u) = -2 \frac{J_0'(\pi u)}{\pi u} = \prod_{l=1}^{\infty} 1 - \left(\frac{u}{\mu_{0,l}} \right)^2 \quad (27)$$

where the factor $B_{0,0}$ has been set to unity so that the value of $F_S(u)$ at the origin is 1.

The model function that Taylor chose is

$$F_M(u) = \begin{cases} \cos\left(\pi\sqrt{u^2 - A^2}\right), & u > A \\ \cosh\left(\pi\sqrt{A^2 - u^2}\right), & u < A \end{cases} \quad (28)$$

which is continuous and has the value 1 at $A = u$. For large u , the function behaves as $\cos \pi u$, and oscillates between plus and minus one, whereas for u approaching zero, tends to $\cosh \pi A$. Thus the peak to sidelobe level ratio is governed by the parameter A^6 , whose value is determined from

$$A = \operatorname{arccosh}(SLL)/\pi \quad (29)$$

⁶At the start of this report A was used for the area of the aperture, but this no longer plays a part in the analysis. Taylor chose A for his design parameter, and we continue with his notation in this section.

where SLL is the design sidelobe level in linear units. Zeros of $F_M(u)$ occur at the points

$$u_m = \pm \sqrt{A^2 + (m - 1/2)^2}, \quad m = 1, 2, 3, \dots \quad (30)$$

Unfortunately $F_M(u)$ is not a realisable antenna pattern, the function oscillates between ± 1 for all u , but u is limited in real space to be less than $2a/\lambda$. Thus this pattern has large reactive energy, which is an undesirable feature in antenna design.

The process now is to start with $F_S(u)$ developed in equation 27, and shift a number, M , of the zeros which are close to the origin to align with the zeros of the model function. Doing this directly leads to a discontinuity in placement at the end of the modified section, resulting in a large sidelobe at this location. However, Taylor showed that by scaling the positions u_m so that the M^{th} zero μ_M of $F_S(u)$ and u_M coincide, this can be avoided. Thus the plan is to construct an entire function with the zeros defined by

$$\pm \sigma u_m, \quad 1 \leq m < M \quad (31)$$

$$\pm \mu_{0,m}, \quad m \geq M \quad (32)$$

where $\sigma = \mu_{0,M}/u_M$, and is referred to as the beam broadening factor [10] as it is a measure of the increase in width of the main beam. Since the zeros are symmetrical about the origin, the modified function can be written in terms of the positive zeros

$$F(u) = -2 \frac{J_0'(\pi u)}{\pi u} \frac{\prod_{m=1}^{M-1} 1 - (u/\sigma u_m)^2}{\prod_{m=1}^{M-1} 1 - (u/\mu_{0,m})^2} \quad (33)$$

This is quite a remarkable result since the antenna radius affects the radiation pattern only through the parameter u , which is proportional to $a \sin \theta$. For a different size antenna with the same design sidelobe level and parameter M , the radiation pattern will simply be scaled in angle by an appropriate change in $\sin \theta$ to keep u constant. Thus accommodating such things as frequency agility in a radar model need not entail complete recalculation of the aperture design parameters, specifically the σu_m and $\mu_{0,m}$, but only a revision of the apparent aspect angle. However, this should not be considered in wideband applications as the optimum choice of the parameter M is a function of the antenna radius [10].

With regard to the above formula, since the M^{th} zeros of the starting function and the scaled model function are identical, the product in the bottom line cancels only the first $M - 1$ zeros, $\mu_{0,m}$, of $J_0'(\pi u)$ and replaces them with the first $M - 1$ zeros, σu_m , of the shifted model function, in the top line. Note that this shifting of the zeros does not modify the peak signal strength of the main lobe of the antenna. Obviously there must be an increase in the aperture field strength to maintain the signal strength because the Taylor weighted antenna will have less gain and lower sidelobes than the uniform aperture distribution.

The blue curves of Figure 5 show two examples of the radiation pattern of an antenna of 10 wavelengths radius ⁷ designed to have a near-in sidelobe level of -35 dB. Superimposed on each figure, in brown, is the radiation pattern of the uniform aperture distribution which is the starting pattern of the Taylor design. The dotted orange line indicates the design sidelobe

⁷A 10 wavelengths radius has been chosen for all the examples in this report. It is not specific to any radar system. The results may be scaled to other antenna sizes using the techniques explained in the text.

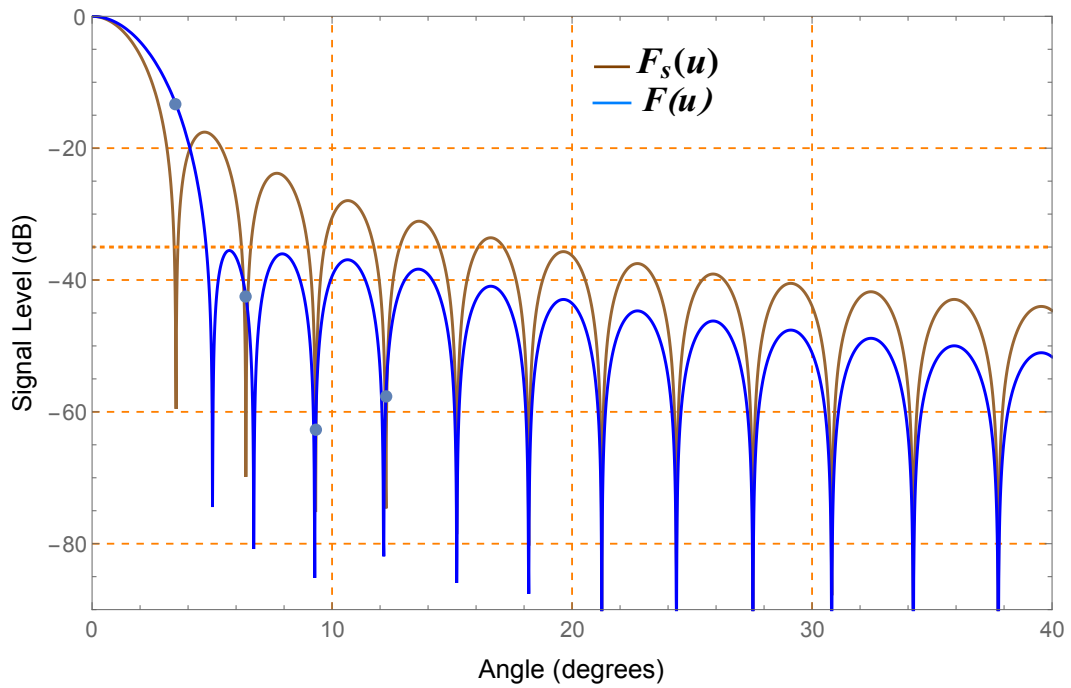
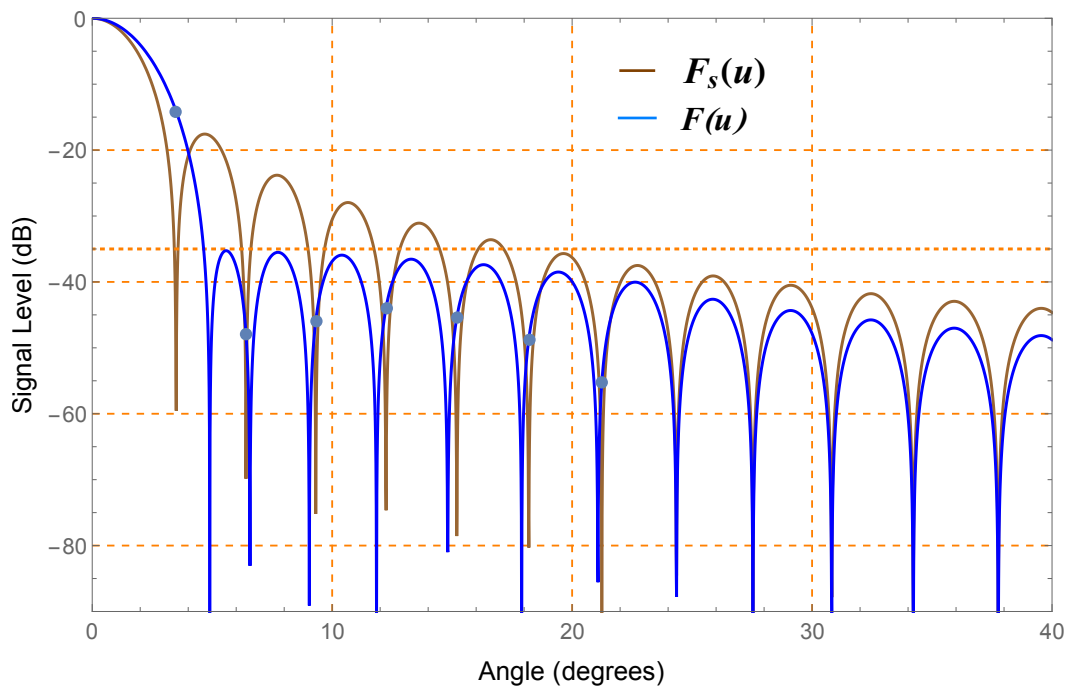
(i) $M=5$ (ii) $M=8$

Figure 5: Taylor radiation pattern for 10 wavelengths radius antenna with -35 dB sidelobes

level. In the top example the parameter, M , has the value 5. The fifth and subsequent nulls of the starting pattern and the final pattern coincide in this example. The first null has the most significant shift, the second somewhat less, but the shifts of the third and fourth are barely discernible on the scale of the figure. Surprisingly, not all of the shifts are in the same direction. Although the model function has uniform sidelobes, the near-in sidelobes of the Taylor distribution have a slight droop with increasing angle, their maxima being, -35.5 dB, -36.1 dB, -36.9 dB and -38.4 dB. Beyond the sidelobes that are shifted, there is also a considerable reduction in sidelobe level from the starting radiation pattern, in this instance being about 8 dB. If the parameter M is increased to 8, shown in the second figure, there is much greater uniformity in the first four sidelobes, there is a droop of only 1.3 dB across them, but the seventh sidelobe is 4.8 dB lower than the first. Beyond this sidelobe, there is a reduction in the subsequent sidelobes of about 4 dB from the uniform radiation pattern. It is interesting to note that the beamwidth in this example is marginally narrower than that of the mainbeam with $M=5$.

Superimposed on both figures are blue dots indicating the points on the Taylor pattern at which $u = \mu_{0,l}$, where $l = 1, \dots, M - 1$ in equation 33. There is a singularity at these points when evaluating equation 33 because both $J_0'(\pi\mu_{0,l})$ and the term $m = l$ of the product in the denominator of equation 33 are equal to 0. This can be avoided by replacing $J_0'(\pi\mu_{0,l})$ by $-J_1(\pi\mu_{0,l})$, then differentiating the numerator and denominator as per l'Hopital's theorem

$$\begin{aligned} \lim_{u \rightarrow \mu_{0,l}} \frac{J_0'(\pi u)}{1 - (u/\mu_{0,l})^2} &= \frac{1}{2} \pi \mu_{0,s} J_1'(\pi \mu_{0,l}) \\ &= \frac{1}{2} \pi \mu_{0,l} J_0(\pi \mu_{0,l}) \end{aligned} \quad (34)$$

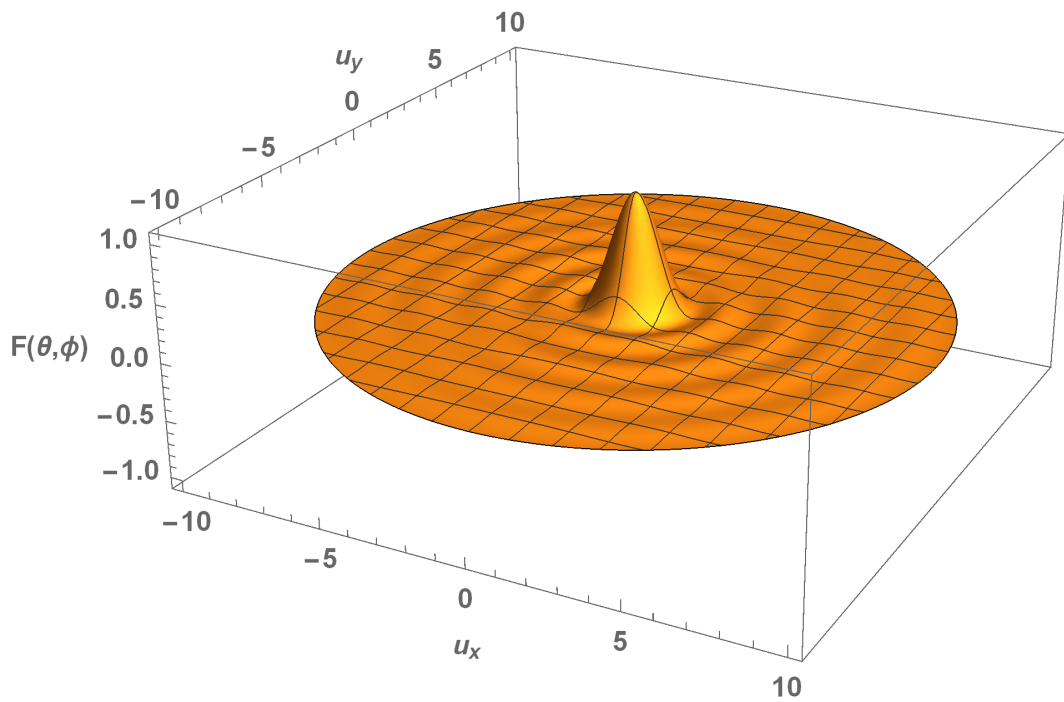
The last line is obtained from the recurrence relationship for $J_1'(z)$ in terms of $J_0(z)$ and $J_1(z)$, (see [9], equation 8.472.1), the latter Bessel function being 0 for $z = \pi\mu_{0,s}$. Thus,

$$F(\mu_{0,l}) = -J_0(\pi\mu_{0,l}) \frac{\prod_{m=1}^{M-1} 1 - (\mu_{0,l}/\sigma u_m)^2}{\prod_{\substack{m=1 \\ m \neq l}}^{M-1} 1 - (\mu_{0,l}/\mu_{0,m})^2}, \quad l = 1, \dots, M - 1 \quad (35)$$

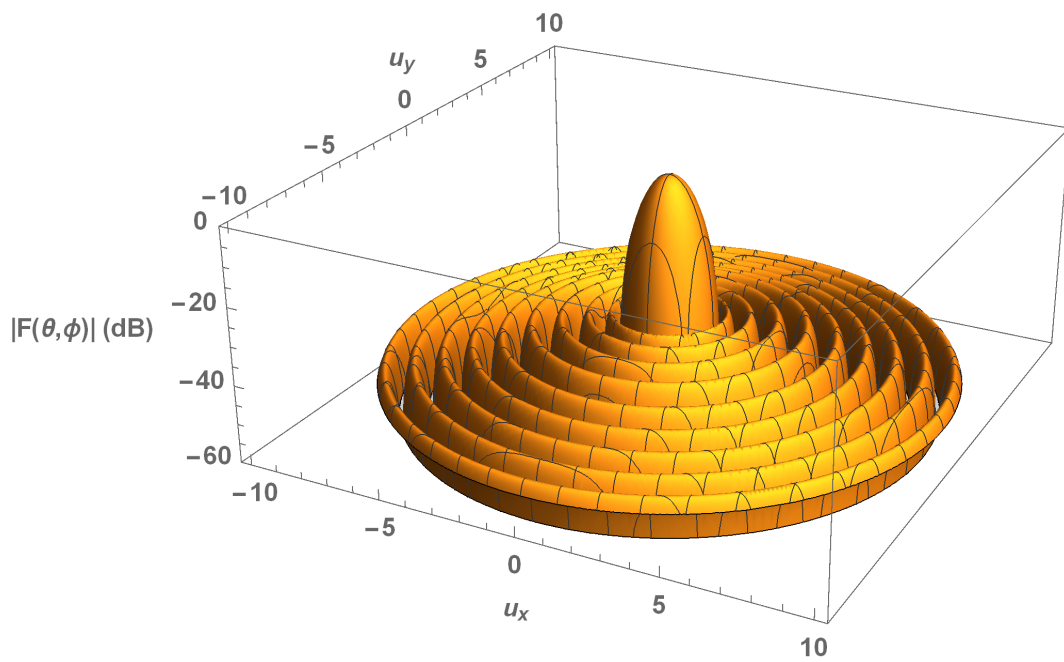
The evaluation of $F(u)$ at these points is also important in the calculation of the coefficients in the expansion of the field in the aperture.

Figure 6 gives two 3 dimensional views of the Taylor radiation pattern for the design of Figure 5(i), which has $M = 5$. The first figure indicates the value of $F(\theta, \phi)$ in the far field of the aperture on a linear scale; this figure is not particularly interesting for the Taylor radiation pattern, having a single peak at the origin reaching a value of 1, but is more insightful for the Bayliss and delta-delta designs to come. The second figure shows $|F(\theta, \phi)|^2$, on a decibel scale, which reveals details of the sidelobe structure of the Taylor design. In the construction of these figures, the radial distance from the centre is the parameter u which covers the range 0 to 10. Since $u = 2a \sin \theta$ the figure includes the radiation pattern from boresight out to an angle of 30 degrees. The angle ϕ is measured anticlockwise from the X axis, corresponding to the line $u_y = 0$ from the centre of the pattern to $u_x = 10$.

We now wish to find the aperture distribution that gives rise to the field specified in equation 33. Since only the term $n = 0$ in equation 13 provides a field independent of ϕ , the aperture



(i) Linear Scale



(ii) decibel Scale

Figure 6: Taylor radiation pattern for 10 wavelengths radius antenna with -35 dB sidelobes, $M = 5$

UNCLASSIFIED

DST-Group-TR-3487

field expansion reduces to

$$E_a(p, \psi) = \sum_{l=0}^{\infty} B_{0,l} J_0(\mu_{0,l} p) \quad (36)$$

With these changes equation 21 becomes

$$F(u) = \frac{2}{\pi^2} \sum_{l=0}^{\infty} B_{0,l} \frac{\pi u J_0(\pi \mu_{0,l}) J_0'(\pi u)}{\mu_{0,l}^2 - u^2} \quad (37)$$

and now the reason for the choice of the zeros of the Bessel functions becomes evident. If we become slightly sloppy with our notation, and evaluate this function at $u = \mu_{0,l'}$, since $J_0'(\pi \mu_{0,l'}) = 0$, all the terms in this summation disappear except for the term $l = l'$ which has a zero in both the numerator and denominator. Thus, on dropping the prime from the l , we are left with

$$\begin{aligned} F(\mu_{0,l}) &= \frac{2}{\pi} B_{0,l} \mu_{0,l} J_0(\pi \mu_{0,l}) \left. \frac{J_0'(\pi u)}{\mu_{0,l}^2 - u^2} \right|_{u \rightarrow \mu_{0,l}} \\ &= B_{0,l} J_0(\pi \mu_{0,l})^2 \end{aligned} \quad (38)$$

where equation 34 has been used in evaluating the limit.

Thus we find from equations 38 and 35 that

$$B_{0,l} = -\frac{1}{J_0(\pi \mu_{0,l})} \frac{\prod_{m=1}^{M-1} 1 - (\mu_{0,l}/\sigma u_m)^2}{\prod_{\substack{m=1 \\ m \neq l}}^{M-1} 1 - (\mu_{0,l}/\mu_{0,m})^2}, \quad l = 1, \dots, M-1 \quad (39)$$

In the expansion of the field in the aperture, there is an additional term $m = 0$ which arises from the singular point $-J_0'(\pi u)/\pi u$ at the origin. The value of $F(0)$ is 1, and hence

$$B_{0,0} = 1 \quad (40)$$

For all l equal to or greater than M , there is no term in the product in the denominator of equation 33 which reduces to zero. Because the associated $\mu_{0,l}$ are zeros of $J_0'(\pi u)$, and are not cancelled by zeros in the denominator, then $F(\mu_{0,l})$ is zero and consequently

$$B_{0,l} = 0, \quad l \geq M \quad (41)$$

Finally, the field distribution in the aperture that produces the desired radiated field is the finite summation

$$E_a(p) = 1 - \sum_{l=1}^{M-1} \frac{J_0(p \mu_{0,l})}{J_0(\pi \mu_{0,l})} \frac{\prod_{m=1}^{M-1} 1 - (\mu_{0,l}/\sigma u_m)^2}{\prod_{\substack{m=1 \\ m \neq l}}^{M-1} 1 - (\mu_{0,l}/\mu_{0,m})^2} \quad (42)$$

Figure 7 shows the aperture distributions which produce the radiation patterns of the two previous examples. Increasing M results in a slight reduction of the field at the centre of the antenna, and a slight upward curve in the field approaching the edge of the aperture.

UNCLASSIFIED

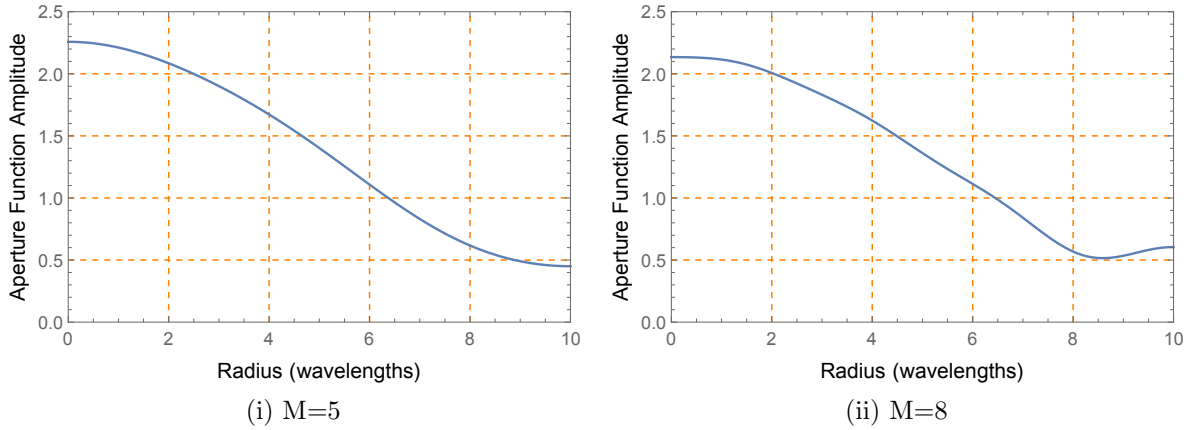


Figure 7: Taylor aperture distribution for 10 wavelengths radius antenna with -35 dB sidelobes

3.3. Bayliss Aperture Distribution

Given that the uniform aperture distribution is the starting point of the Taylor design, it might be reasonable to assume that the design of difference beams would start with a uniform amplitude aperture in which the field is oppositely directed on two halves. With this aperture field, the radiation pattern is of the form

$$\begin{aligned}
 F(\theta, \phi) &= \frac{1}{\pi a^2} \int_0^a \int_0^\pi \rho (e^{j\rho u \cos(\phi-\psi)} - e^{j\rho u \cos(\phi-\psi+\pi)}) d\psi d\rho \\
 &= \frac{2j}{\pi a^2} \int_0^a \int_0^\pi \rho \sin(k\rho \sin\theta \cos(\phi-\psi)) d\psi d\rho
 \end{aligned} \tag{43}$$

In the special cases of $\phi = 0$ or π , the integral reduces to 0, as expected on the plane of symmetry. For the case of $\phi = \pi/2$, with the introduction, as before, of $p = \pi a/\rho$ and $u = 2a \sin\theta$,

$$\begin{aligned}
 F(\theta, \pi/2) &= \frac{2j}{\pi^3} \int_0^\pi \int_0^\pi p \sin(pu \sin\psi) d\psi dp \\
 &= \frac{2j}{\pi^2} \int_0^\pi p H_0(pu) dp \\
 &= 2j \frac{H_1(\pi u)}{\pi u}
 \end{aligned} \tag{44}$$

where $H_1(z)$ is the Struve function of the first kind, order 1, argument z . A plot of this function is shown in Figure 8. It looks promising, the peak signal is at $u = 0.84$, and is 3.19 dB less than the peak of the uniform aperture⁸ but the function has no real zeros except at the origin, and thus is not amenable to Taylor's technique.

In equation 13, a general formula for describing the aperture field is provided in terms of a Fourier Bessel series expansion. To describe the field of two oppositely directed uniform half

⁸Kinsey [12] states that the maximum signal level of a difference beam is -2.47 dB for a circular aperture, which differs from the figure above

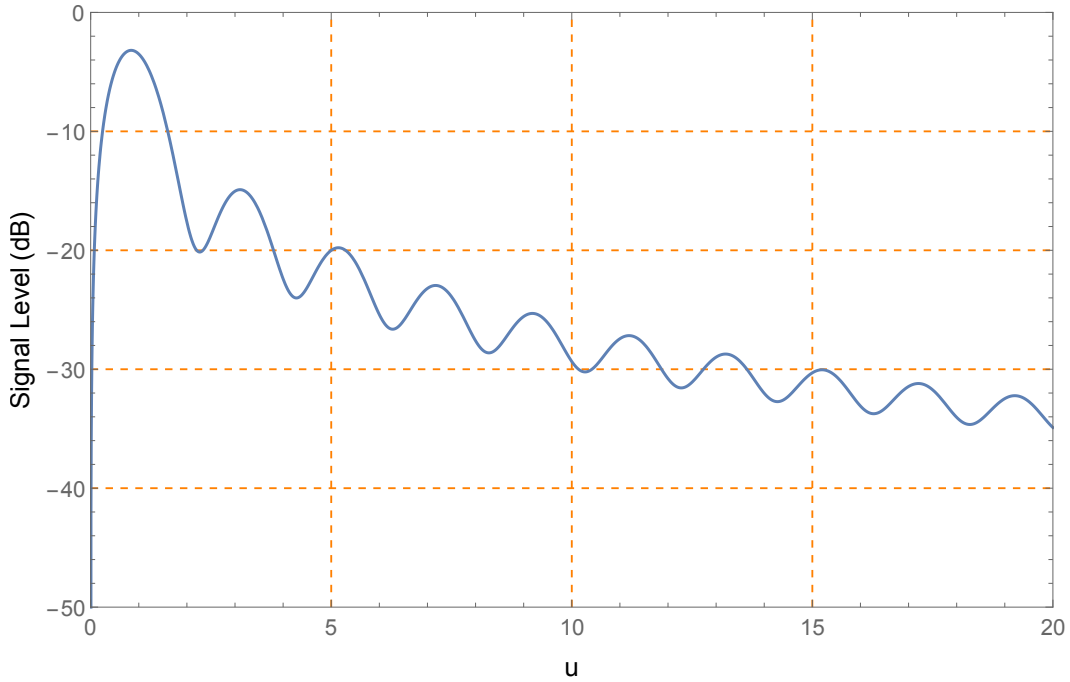


Figure 8: Uniform difference beam radiation pattern

apertures above would require a very large number of Fourier components. However, all one requires to generate suitable difference beams is for the fields in the opposing halves to be of opposite sign, and be zero on the plane of symmetry, and this can be achieved with the terms $n = \pm 1$ of equation 13 with an appropriate choice of $B_{1,l}$ and $B_{-1,l}$. Thus

$$\begin{aligned} E_a(p, \psi) &= \sum_{l=0}^{\infty} B_{1,l} e^{j\psi} J_1(\mu_{1,l} p) + B_{-1,l} e^{-j\psi} J_{-1}(\mu_{-1,l} p) \\ &= \sum_{l=0}^{\infty} (B_{1,l} e^{j\psi} - B_{-1,l} e^{-j\psi}) J_1(\mu_{1,l} p) \end{aligned} \quad (45)$$

since $J_1(z) = -J_{-1}(z)$ and their zeros are identical (see [1], equation 9.1.5). If we wish to generate an azimuth monopulse beam (with reference to the x axis of figure 1), then the first and second quadrants need to be in phase, and the third and fourth of opposite phase to the former two, whereas for an elevation monopulse beam the first and fourth quadrants need to be in phase, and the second and third of opposite phase. Thus for the azimuth beam, choosing $B_{1,l} = B_{-1,l}$, and recalling that ψ is measured from the x axis (Figure 1),

$$E_a(p, \psi) = 2j \sin \psi \sum_{l=0}^{\infty} B_{1,l} J_1(\mu_{1,l} p) \quad (46)$$

and for the elevation beam, with $B_{-1,l} = -B_{1,l}$,

$$E_a(p, \psi) = 2 \cos \psi \sum_{l=0}^{\infty} B_{1,l} J_1(\mu_{1,l} p) \quad (47)$$

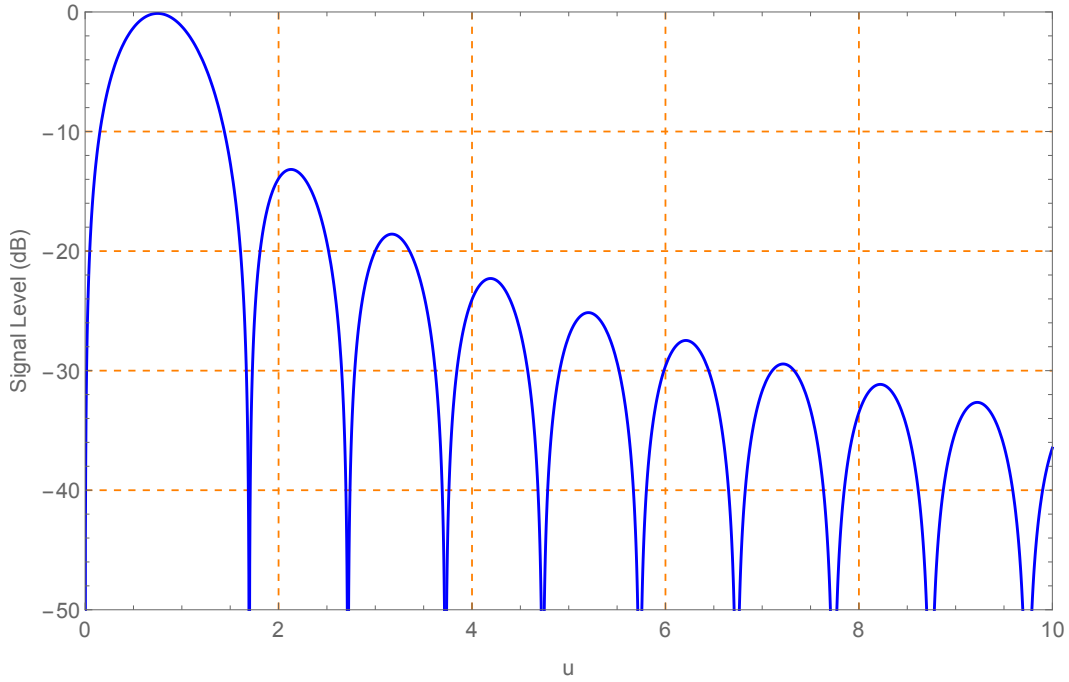


Figure 9: Plot of $\pi u J_1'(\pi u)/(1.0 - (u/\mu_{1,1}))^2$ normalised to 1

The radial distribution components of both beams are identical, the angular modulation by $\sin \psi$ or $\cos \psi$ determining the use to which the beam is to be put. Whereas Bayliss chose to use only the $n = \pm 1$ terms, in fact the terms $n = \pm 3, \pm 5, \dots$ would also satisfy the phase requirements around the aperture; we will not investigate these terms, but their inclusion could be beneficial in improving the monopulse signal gain. Note the presence of the term j in the azimuth beam; this indicates an advancement in phase of 90° in the azimuth monopulse beam relative to the elevation monopulse beam.

With $n = \pm 1$, the first term of equation 21 for the expansion of $F(\theta, \phi)$ of the elevation beam is

$$\frac{4}{\pi^2} \cos \phi B_{1,1} \frac{\pi u J_1(\pi \mu_{1,1}) J_1'(\pi u)}{\mu_{1,1}^2 - u^2} \quad (48)$$

and is expected to be the most significant term of $F(u, \phi)$. Thus, an appropriate starting point to generate the low sidelobe elevation monopulse beam is the function

$$F_S(u) = C_1 \pi u J_1'(\pi u)/(1.0 - (u/\mu_{1,1}))^2 \quad (49)$$

in which the numerator adds a zero, u , at the origin, and the denominator removes the first zero of $J_1'(\pi u)$. Incorporation of $\cos \phi$ or $\sin \phi$ in this expression generates the angular dependence of the elevation and azimuth beams. C_1 is a constant to be applied retrospectively, to set the peak value of the final beam $F(u)$ at a convenient amplitude, in our case unity. Figure 9 shows the behaviour of the starting function for u up to 10.0. This function is an entire function with real zeros, and is expressible as an infinite product ([1], equation 9.5.11).

Bayliss [3] showed that a low sidelobe difference beam could be generated using the derivative

of the ideal Taylor function as a starting point. Recalling that in the Taylor design

$$F_M(u) = \frac{1}{\pi} \cos\left(\pi\sqrt{u^2 - A^2}\right) \quad (50)$$

where we have introduced an additional factor $1/\pi$, then the Bayliss design is

$$F_M(u) = u \frac{\sin\left(\pi\sqrt{u^2 - A^2}\right)}{\sqrt{u^2 - A^2}} \quad (51)$$

For large u , this expression is asymptotic to $\sin \pi u$, and thus oscillates between plus and minus one. Unlike the Taylor model function, the maximum value of $F_M(u)$ does not occur at the origin, and hence is a function of both A and u . It is complicated to determine the value of A for a specified sidelobe ratio; at the peak, A and u are related by the transcendental equation

$$\tanh\left(\pi\sqrt{A^2 - u^2}\right) = \pi \frac{u^2}{A^2} \sqrt{A^2 - u^2} \quad (52)$$

but this does not have a simple solution for u in terms of A . However, using an iterative procedure in *Mathematica*, it is relatively straightforward to determine the value of A to give the required sidelobe level, and the associated value of u . The zeros of $F_M(u)$ occur at

$$u_m = \pm\sqrt{A^2 + m^2}, \quad m = 1, 2, 3, \dots \quad (53)$$

However, Bayliss noted that using this approach, the first few sidelobes were slightly higher than the intended design level, and found through a parametric study that by adjusting the first four zeros and the value of A , much closer results to the design sidelobe levels could be obtained. He summarised his results as a set of polynomial coefficients that could be used to evaluate A and the four zero positions $\xi_1, \xi_2, \xi_3, \xi_4$ that needed to be shifted. Elliott [7] published tables of these parameters for design sidelobe levels from -15 dB to -40 dB in 5 dB increments, and it is these tables which are currently implemented in our software. Figure 10 shows a comparison of the model function described above for a -30 dB sidelobe design, in red, with the modified parameters of Bayliss' final design, in blue. It can be seen that the first four sidelobes have been reduced very closely to the design sidelobe level. The interrelationship of A and the ξ parameters is quite complex. The value of A found for the model function is 1.722, whereas the optimum value when the zeros are shifted is 1.641.

In summary, the zeros of the model function are at

$$u_m = \begin{cases} 0, & m = 0 \\ \pm\xi_m, & m = 1, 2, 3, 4 \\ \pm\sqrt{A^2 + m^2}, & m = 5, \dots, M \end{cases} \quad (54)$$

The process then is much the same as developed by Taylor. The M zeros u_m are scaled by a factor σ so that u_M coincides with $\mu_{1,M+1}$, the $M + 1^{\text{th}}$ zero of $J_1(\pi\mu)$, i.e.

$$\sigma = \frac{\mu_{M+1}}{u_M} \quad (55)$$

The first M zeros of $J_1'(\pi u)$ in equation 49 are removed (the first one, which falls within the main beam of the radiation pattern, has already been removed by the term $(1.0 - (u/\mu_{1,1})^2)$

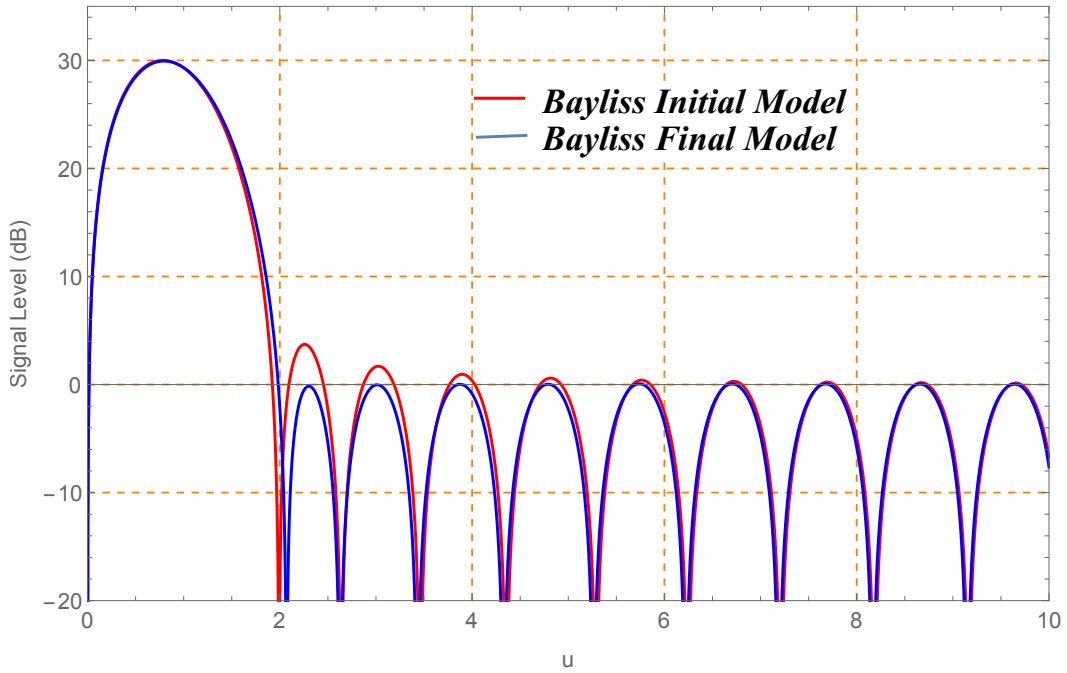


Figure 10: Comparison of ideal model with Bayliss modified zero placement for -30 dB sidelobes

in the denominator) and replaced by the $M - 1$ zeros σu_m . and are scaled by the factor σ as described above. The final result of shifting these zeros is

$$F(u) = C_1 \left\{ \begin{array}{c} \sin \phi \\ \cos \phi \end{array} \right\} \pi u J_1'(\pi u) \frac{\prod_{m=1}^{M-1} 1 - (u/\sigma u_m)^2}{\prod_{m=1}^M 1 - (u/\mu_{1,m})^2} \quad (56)$$

with $\sin \phi$ for the azimuth beam, the $\cos \phi$ for the elevation beam.

Figure 11 shows the radiation patterns of two monopulse beam designs for a 10 wavelength radius antenna with -30 dB sidelobes, the final function in blue and the starting function in brown. The orange dotted line indicates the design sidelobe level. In both figures, the cut is through the peak of the radiation pattern, which has been normalised to unity (0 dB). In the first subfigure, $M = 5$, i.e. the first four nulls are shifted as per Bayliss's calculations, and the nulls up to and including the fifth null are scaled such that the fifth null (u_5) coincides with the sixth null ($\mu_{1,6}$) of $J_1'(\pi u)$. Because of the effect of shifting the first null significantly to the right in the figure, the main lobe is increased in magnitude from the starting function, and the maximum occurs at a slightly greater angle. The near-in sidelobe levels are -30.7 dB, -31.05 dB, -31.8 dB, and -33 dB, indicating that a general droop still exists across the region Bayliss sought to improve. With $M = 8$, the second subfigure of Figure 11, the peak of the main beam is reduced slightly in amplitude, and occurs at a very slightly reduced angle, but the sidelobes are more uniform. The values of the first four sidelobes are -30.7 dB, -30.6 dB, -30.9, and -31.5 dB; after the third sidelobe they drop away more rapidly, and after the seventh, follow closely the fall rate of the starting function.

Figure 12 gives a perspective view of the Bayliss design radiation pattern for the case $M = 5$ with -30 dB sidelobes. In the upper figure, which uses a linear scale, in the angular range

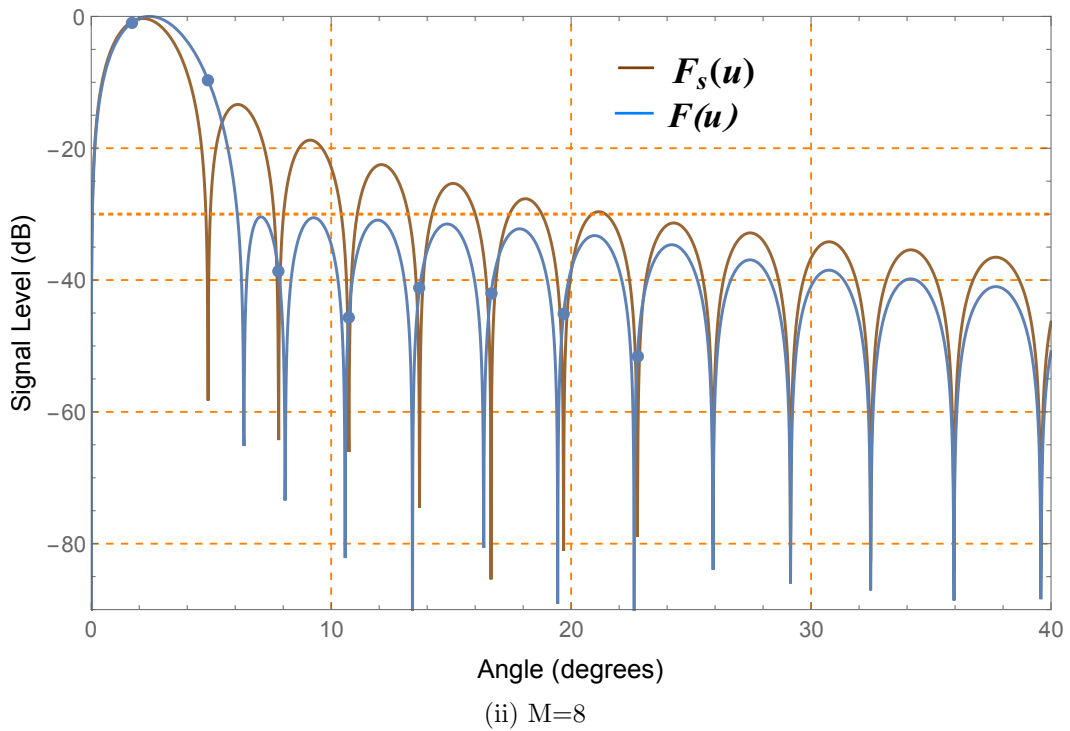
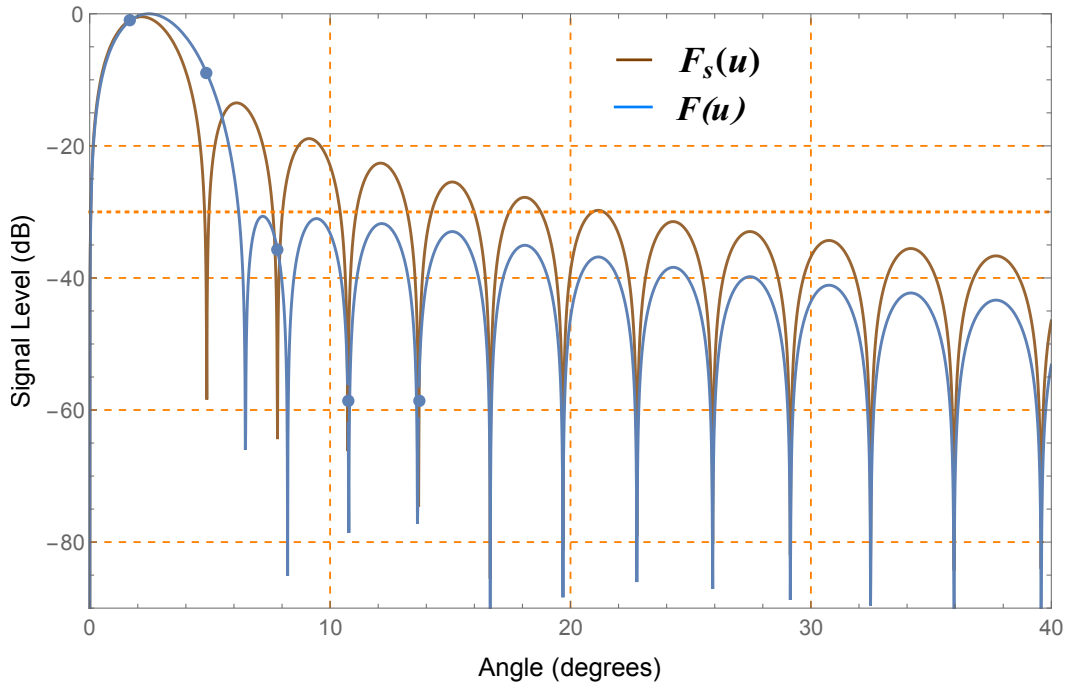
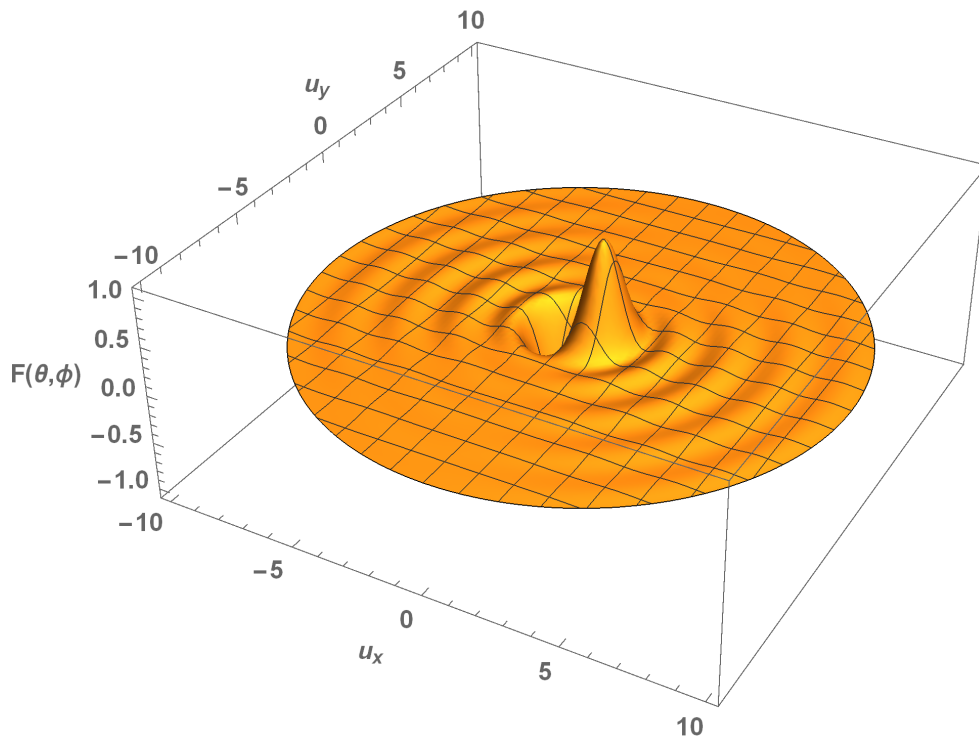
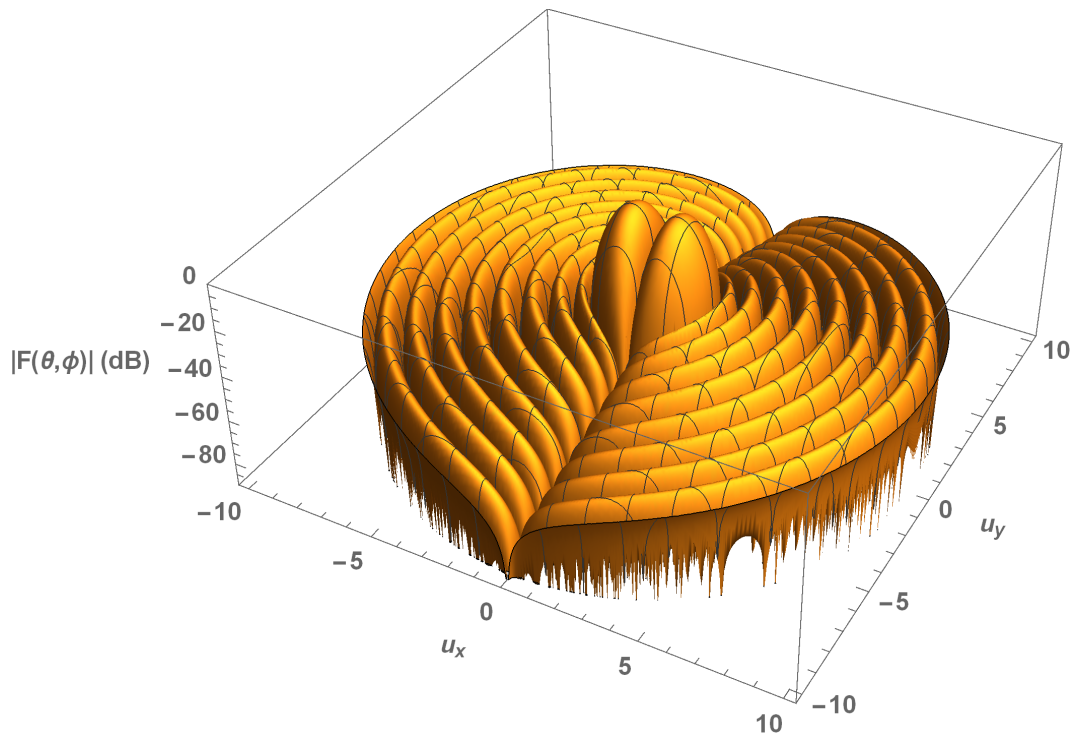


Figure 11: Comparison of Bayliss and starting function radiation patterns in the plane $\phi = 90^\circ$ for a 10 wavelengths radius antenna with -30 dB sidelobes



(i) Linear Scale



(ii) decibel Scale

Figure 12: Perspective views of Bayliss radiation pattern for 10 wavelengths radius antenna with -30 dB sidelobes, $M = 5$

UNCLASSIFIED

DST-Group-TR-3487

0 to π the field strength is positive directed and there is a peak of unit amplitude at $\pi/2$, whereas in the range π to 2π there is a similar peak, but it is negatively directed and hidden by the disc of sidelobes. The presence of the negative peak is intimated by the depression to the left of the positive peak. Small ripples in the disk of this figure indicate the sidelobes of the radiation pattern, fading to nothing at 0 and π , but they are much more pronounced in the lower figure which plots the absolute value of the field strength on a decibel scale. The deep null running across this pattern, barely discernible in the upper figure, marks the plane of symmetry of the Bayliss radiation pattern.

The same problem with the Bayliss design is experienced when evaluating $F(u)$ at the points $u = \mu_{1,l}$ as occurred with the Taylor design. Again, using l'Hopital's theorem,

$$\begin{aligned} \lim_{u \rightarrow \mu_{1,l}} \frac{J_1'(\pi u)}{1 - (u/\mu_{1,l})^2} &= -\pi \mu_{1,l} J_1''(\pi \mu_{1,l})/2 \\ &= \pi \mu_{1,l} \left(1 - \frac{1}{\pi^2 \mu_{1,l}^2}\right) J_1(\pi \mu_{1,l})/2 \end{aligned} \quad (57)$$

in which we have made use of the differential equation for $J_1(z)$ evaluated at $z = \pi\mu$, viz.

$$\pi^2 \mu^2 J_1''(\pi\mu) + \pi\mu J_1'(\pi\mu) + (\pi^2 \mu^2 - 1) J_1(\pi\mu) = 0 \quad (58)$$

and $J_1'(\pi\mu)$ is identically zero for $\mu = \mu_{1,l}$. Thus

$$F(\mu_{1,l}) = \frac{C_1}{2} (\pi^2 \mu_{1,l}^2 - 1) J_1(\pi \mu_{1,l}) \frac{\prod_{m=1}^{M-1} 1 - (\mu_{1,l}/\sigma u_m)^2}{\prod_{\substack{m=1 \\ m \neq l}}^M 1 - (\mu_{1,l}/\mu_{1,m})^2}, \quad l = 1, \dots, M-1 \quad (59)$$

We now wish to develop an alternative expression for the field in terms of the aperture field, which can then be solved for the parameters $B_{1,l}$. Substituting $u = \mu_{1,l}$ in equation 21, for the Bayliss design with $n = \pm 1$, all of the terms in the summation over l are zero except for the term $l = l'$, and consequently $F(\mu_{1,l'})$ is only a function of $B_{1,l'}$, thus, (and dropping the prime from l'),

$$\begin{aligned} F(\mu_{1,l}) &= \frac{4}{\pi^2} B_{1,l} \pi \mu_{1,l} J_1(\pi \mu_{1,l}) \frac{J_1'(\pi u)}{\mu_{1,l}^2 - u^2} \Bigg|_{u \rightarrow \mu_{1,l}} \\ &= 2 B_{1,l} J_1(\pi \mu_{1,l})^2 \left\{ 1 - \frac{1}{\pi^2 \mu_{1,l}^2} \right\} \end{aligned} \quad (60)$$

in which we have made use of equation 57. Thus we find that

$$B_{1,l} = \frac{C_1}{4} \frac{\pi^2 \mu_{1,l}^2}{J_1(\pi \mu_{1,l})} \frac{\prod_{m=1}^{M-1} 1 - (\mu_{1,l}/\sigma u_m)^2}{\prod_{\substack{m=1 \\ m \neq l}}^M 1 - (\mu_{1,l}/\mu_{1,m})^2}, \quad l = 1, \dots, M-1 \quad (61)$$

and

$$E_a(p, \psi) = \frac{C_1}{4} \cos \psi \sum_{l=0}^{M-1} \pi^2 \mu_{1,m}^2 \frac{J_1(p \mu_{1,l})}{J_1(\pi \mu_{1,l})} \frac{\prod_{m=1}^{M-1} 1 - (\mu_{1,l}/\sigma u_m)^2}{\prod_{\substack{m=1 \\ m \neq l}}^M 1 - (\mu_{1,l}/\mu_{1,m})^2} \quad (62)$$

UNCLASSIFIED

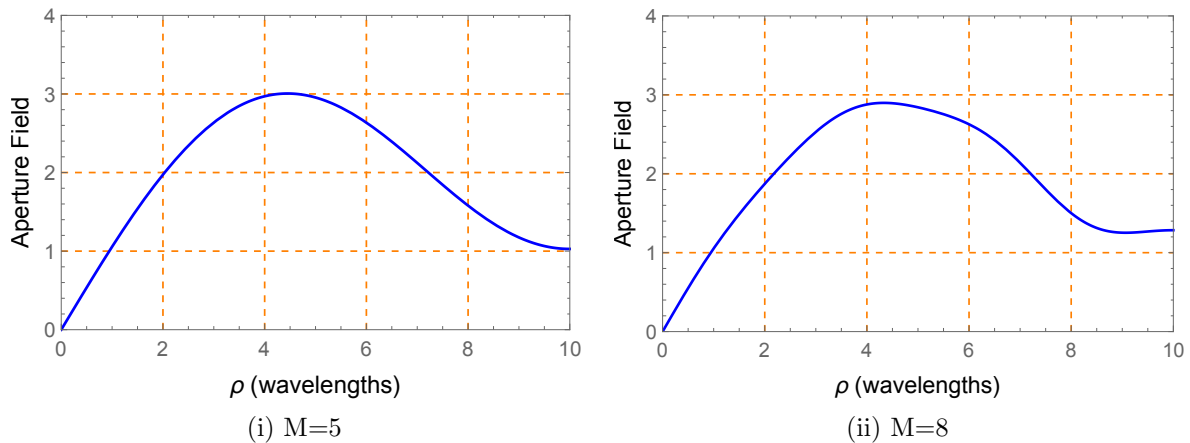


Figure 13: Bayliss aperture distribution in the plane $\psi = 90^\circ$ for a 10 wavelengths radius antenna with -30 dB sidelobes

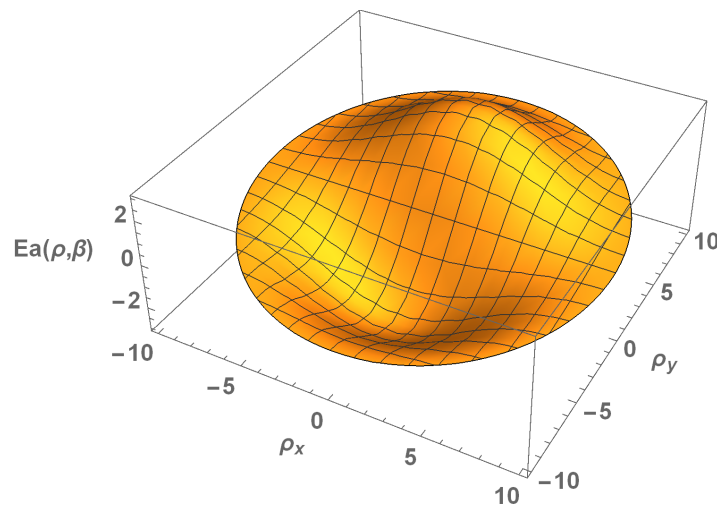


Figure 14: Perspective view of the aperture distribution of Figure 13(i)

Figure 13 shows the peak values, as a function of ρ at $\psi = \pi/2$, of the aperture distribution functions that produce the radiation patterns of the two previous examples. In the first case, $M = 5$, the aperture field is zero at the centre, and peaks at a value of almost precisely 3 at a radius of 4.45 wavelengths from the centre, before tapering to 1.03 at the edge of the aperture. With $M = 8$, the maximum reduces slightly to 3.9 at 4.33 wavelengths from the centre, but there is a small hump as the field strength reduces towards the edge of the aperture before turning upwards slightly to a value of 1.28 at the aperture edge. Figure 14 shows a perspective view of the current distribution over the whole aperture, for the case $M = 5$, highlighting the variation in field strength with angle ψ . The coordinate axes ρ_x and ρ_y indicate the projection of the radial ρ onto the X and Y axes. The cuts in Figure 13 correspond to the line $\rho_x = 0$, $0 < \rho_y < 10$ of Figure 14. The difference between the two current distributions of Figure 13 is not discernible on the scale of this figure.

3.4. Delta-Delta Aperture Distribution

The delta-delta beam ideally has nulls on both the X and Y axes of figure 1, to coincide with the nulls of the azimuth and elevation difference beams, and any aperture field generating this radiation pattern must perforce be of the form $\sin(2\psi)$ (or $\cos(2\psi)$), or a combination of odd harmonic multiples of this. The design by Chesley [5] utilises only the terms $n = \pm 2$ of equation 13, which reduces it to

$$\begin{aligned} E_a(p, \psi) &= \sum_{l=0}^{\infty} B_{2,l} e^{j2\psi} J_2(\mu_{2,l} p) + B_{-2,l} e^{-j2\psi} J_{-2}(\mu_{-2,l} p) \\ &= 2j \sin(2\psi) \sum_{l=0}^{\infty} B_{2,l} J_2(\mu_{2,l} p) \end{aligned} \quad (63)$$

where we have used $J_{-2}(z) = J_2(z)$ ([1], equation 9.1.5), and set $B_{-2,l} = -B_{2,l}$. The term j indicates a 90° phase shift of the delta-delta beam and will be ignored.

In the expression for $F(\theta, \phi)$ in terms of the aperture function, equation 21, the term with $l = 1$ is expected to be the most significant contributor to the total field and is of the form

$$\frac{4}{\pi^2} \sin(2\phi) B_{2,1} \frac{\pi u J_2(\pi \mu_{2,1}) J_2'(\pi u)}{\mu_{2,1}^2 - u^2} \quad (64)$$

Thus an appropriate form of the field to start with to generate the double difference field is

$$F_S(u) = C_2 \frac{\pi u J_2'(\pi u)}{1 - (u/\mu_{2,1})^2} \quad (65)$$

where C_2 is a constant to set the maximum value of the function $F(u)$ to unity, and is multiplied by $\sin(2\phi)$ to provide the angular variation in the aperture field. The first twenty zeros $\mu_{2,l}$ of $J_2'(\pi u)$ are listed in Table 1. Figure 15 compares $J_2(\pi u)$, in red, $\pi J_2'(\pi u)$, in blue, and the starting function, with $C_2 = 1$, in green. What is important to note is that the derivative of $J_2(\pi u)$ is zero at the origin, and the extra term u in the starting function provides an extra zero at the origin. Also, in this last curve, the first zero of $J_2'(\pi u)$ has been removed by the term $1 - (u/\mu_{2,1})^2$ in the denominator of the expression, but all other zeros coincide with the zeros of the red curve. Thus the entire function whose zeros are defined by $l = \pm 2, \pm 3, \dots$ is

$$F_S(u) = C_2 \prod_{l=2}^{\infty} 1 - \left(\frac{u}{\mu_{2,l}} \right)^2 \quad (66)$$

Chesley's choice of a model function for the delta-delta beam is derived from Taylor's design for the sum beam. It must be an even function of u with the value zero at the origin, have uniform sidelobes and a minimum beamwidth for a given peak-to-sidelobe ratio. Chesley found that subtracting two Taylor model functions, with an appropriate scale parameter to produce a zero at $u = 0$, satisfies these requirements, thus

$$F_M(u) = \cos \pi \sqrt{u^2 - A_1^2} - K \cos \pi \sqrt{u^2 - A_2^2} \quad (67)$$

As with the Taylor design, the \cos terms change to \cosh when the arguments within their respective square root signs are negative, and the functions are continuous where the values

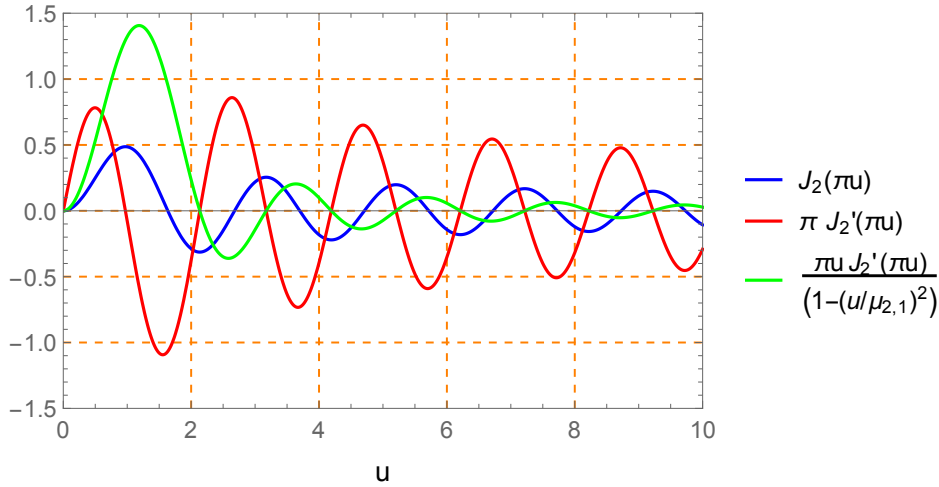


Figure 15: Comparison of $J_2(\pi u)$, $\pi J_2'(\pi u)$, and the starting function for the delta-delta antenna radiation pattern

of their arguments are zero. At $u = 0$, the cosine functions take the values $\cosh(\pi A_1)$ and $\cosh(\pi A_2)$, and thus selecting

$$K = \frac{\cosh(\pi A_1)}{\cosh(\pi A_2)} \quad (68)$$

ensures a zero at the origin. Since both cosine terms oscillate between ± 1 for large u , selection of a suitably large K , which implies that A_2 is smaller than A_1 , ensures that the second term dominates the setting of the sidelobe level. A value of K of 10 (20 dB) results in a variation of the combined sidelobe level between +0.8 dB to -0.9 dB compared with the second term sidelobe level, and was considered an appropriate design parameter by Chesley [5]. Since typical values of A_1 and A_2 are 2 or greater, K is approximately given by

$$K \approx e^{\pi(A_1 - A_2)} \quad (69)$$

Thus for $K = 10$, the difference between A_1 and A_2 should be about 0.73. It is not particularly clear though how to design for the peak of the main beam except by trial and error, since this is obtained as the difference of two nearly equal terms. Chesley [5] recommends that to achieve a specified sidelobe level, the sidelobe level of the first term should be set at the design value minus 40 dB, and for the second term at the design value minus 20 dB, and this gives results within about 1 dB of the design goal. In Figure 16 we illustrate the interaction of the terms for a design sidelobe level of -30 dB. The design begins with A_1 and A_2 appropriate, respectively, for -70 dB and -50 dB sidelobe levels, but it was found by trial and error that setting the levels to -68 dB and -48 dB put the first sidelobe at precisely -30 dB, and this is illustrated in the figure. The red curve corresponds to the first term of equation 67, and the green curve to the second term. It is impossible to judge by eye where the difference between these curves is greatest as they are plotted on a logarithmic scale. The blue curve shows this difference, the intended model function. The curves are scaled so that the peak value of the difference is precisely unity (0 dB). The first sidelobe of the second term (green) is consumed by the mainlobe of the first term (red), but the remaining sidelobes of the second term control the sidelobes of the model function. It is apparent that some experimentation is required in developing a satisfactory design.

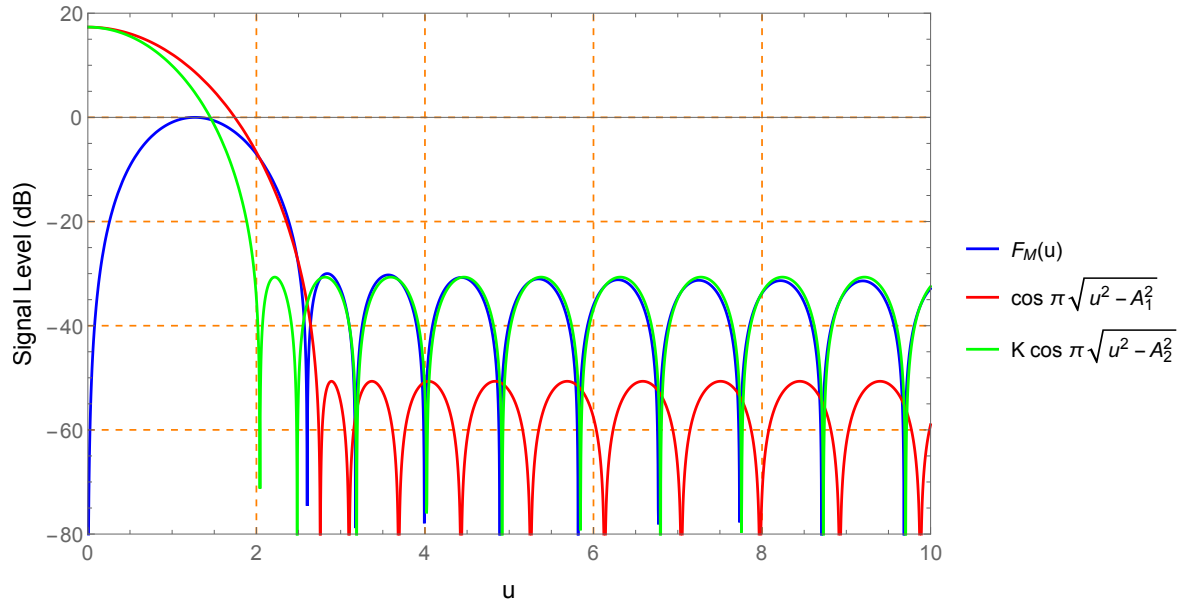


Figure 16: Comparison of terms contributing to the delta-delta model function

The positions of the first M zeros of the model function need to be determined. The zeros of the second term of the model function are at the zeros of the cos function

$$\begin{aligned} \pi \sqrt{u^2 - A_2^2} &= \frac{\pi}{2}, \frac{3\pi}{2}, \frac{5\pi}{2}, \dots \\ &= \pi \left(m - \frac{1}{2} \right), \quad m = 1, 2, 3, \dots \end{aligned} \quad (70)$$

However, the first null is subsumed by the main beam (see figure 16) and the nulls that are retained are located at

$$u_m = \sqrt{A_2^2 + (m + 1/2)^2}, \quad m = 1, 2, 3, \dots \quad (71)$$

As there are subtle changes in position of the nulls of the resulting model function due to the influence of the first term, Chesley uses a single step procedure using Newton's method to refine the positions of the zeros in the model function, beginning with the above points. However, it is much simpler and more accurate to use the `FindRoot` function of *Mathematica* with the above points as the starting points for the function. In the subsequent discussion, we assume that the zeros u_m are the refined positions provided by `FindRoot`.

Again we are faced with the problem that the model function is not a suitable antenna pattern because it does not diminish suitably with large u , and the process to be implemented is the same as for the previous two designs. Starting with the expansion of $F_S(u)$ in terms of its zeros, because the first zero lies within the main beam, the zeros of the model function are scaled so that the M^{th} zero coincides with the $M + 1^{\text{th}}$ zero of $F_S(u)$. The scale factor is therefore

$$\sigma = \frac{\mu_{2,M+1}}{u_M} \quad (72)$$

Thus the zeros from 2 to M of $F_S(u)$ are replaced with the $M - 1$ terms σu_m . After a little

rearranging of the expression we find that

$$F(u) = C_2 \pi u J_2'(\pi u) \frac{\prod_{m=1}^{M-1} 1 - (u/\sigma u_m)^2}{\prod_{m=1}^M 1 - (u/\mu_{2,m})^2} \quad (73)$$

Note that the denominator of the fraction in equation 65 has been incorporated in the product term in the denominator of equation 73. It follows that the radiation pattern as a function of ϕ is

$$F(\theta, \phi) = \sin 2\phi F(u) \quad (74)$$

Figure 17 shows the radiation patterns of two delta delta designs in the plane $\phi = 45^\circ$, both with a -30 dB design sidelobe level for an antenna of 10 wavelengths radius. In the upper figure, $M = 5$, the fifth and subsequent nulls of the starting function and the final design coincide, whereas in the lower figure, with $M = 8$, the eighth and subsequent nulls coincide. Apart from the first two nulls in each figure, the shift of the nulls is relatively minor to achieve the required radiation pattern. The parameters $A1$ and $A2$ are evaluated with sidelobe levels of -68 dB and -48 dB, respectively, as, following earlier remarks, with these values the first sidelobe of the model function more closely complies with the design value than the initial recommendation of Chesley. For the upper figure, $M = 5$, the first four sidelobes are at -30.77 dB, -31.06 dB, -32.08 dB, and -33.12 dB, whereas for the lower they are slightly closer, -30.32 dB, -30.86 dB, -31.69 dB and -32.46 dB, to the design sidelobe level. The blue dots on the curves indicate the points $u = \mu_{2,l}$ which are used in calculating the field in the aperture.

For the special case of $u = \mu_{2,m}$ used in the determination of the coefficients in the expansion of the aperture function to generate the desired radiation pattern, we again use l'Hopital's rule to evaluate the limit

$$\begin{aligned} \lim_{u \rightarrow \mu_{2,l}} \frac{J_2'(\pi u)}{1 - (u/\mu_{2,l})^2} &= -\pi \mu_{2,l} J_2''(\pi \mu_{2,l})/2 \\ &= \pi \mu_{2,l} \left(1 - \frac{4}{\pi^2 \mu_{2,l}^2}\right) J_2(\pi \mu_{2,l})/2 \end{aligned} \quad (75)$$

in which we have made use of the differential equation for $J_2(z)$ evaluated at $z = \pi\mu$, viz.

$$\pi^2 \mu^2 J_2''(\pi\mu) + \pi\mu J_2'(\pi\mu) + (\pi^2 \mu^2 - 4) J_2(\pi\mu) = 0 \quad (76)$$

and $J_2'(\pi\mu)$ is identically zero for $\mu = \mu_{2,m}$. Thus

$$F(\mu_{2,l}) = \frac{C}{2} (\pi^2 \mu_{2,l}^2 - 4) J_2(\pi \mu_{2,l}) \frac{\prod_{m=1}^{M-1} 1 - (\mu_{2,l}/\sigma u_m)^2}{\prod_{\substack{m=1 \\ m \neq l}}^M 1 - (\mu_{2,l}/\mu_{2,m})^2}, \quad l = 1, \dots, M-1 \quad (77)$$

Figure 18 shows two perspective views of the radiation pattern of the Chesley design for the example $M = 5$ introduced above. The uppermost figure, with a linear scale, displays four peaks, two positive and two negative, alternating at odd multiples of $\pi/4$ with nulls at multiples of $\pi/2$. The lower figure shows the absolute value of the radiation pattern on a decibel scale. In this figure the nulls are much more discernible.

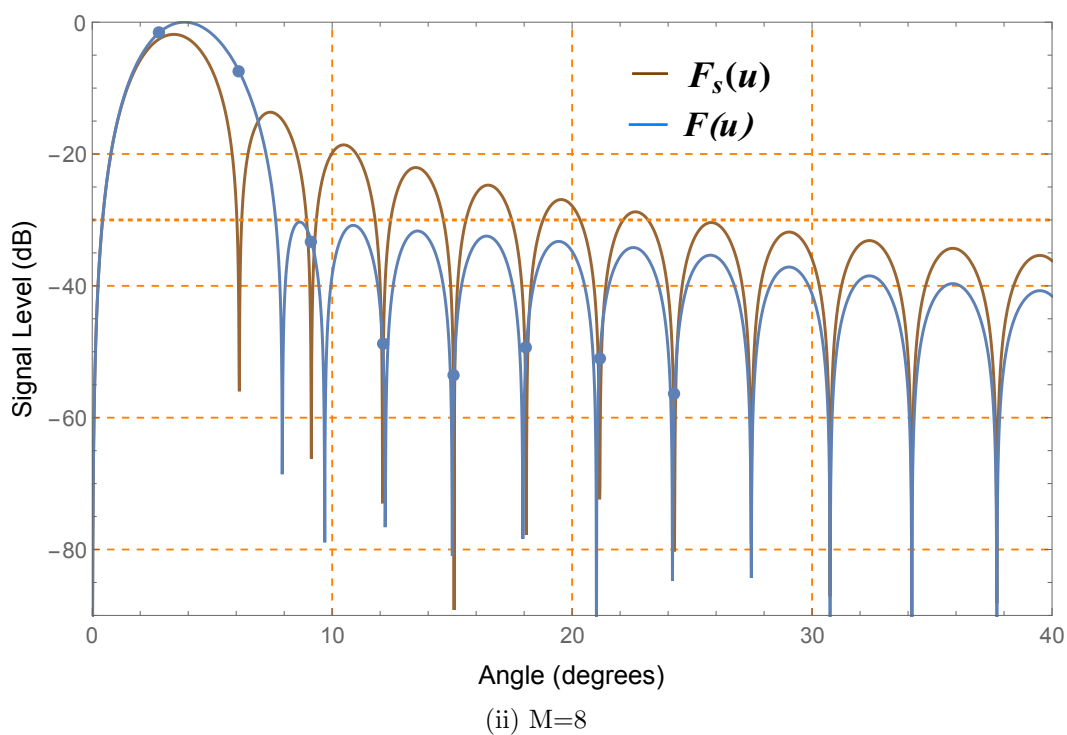
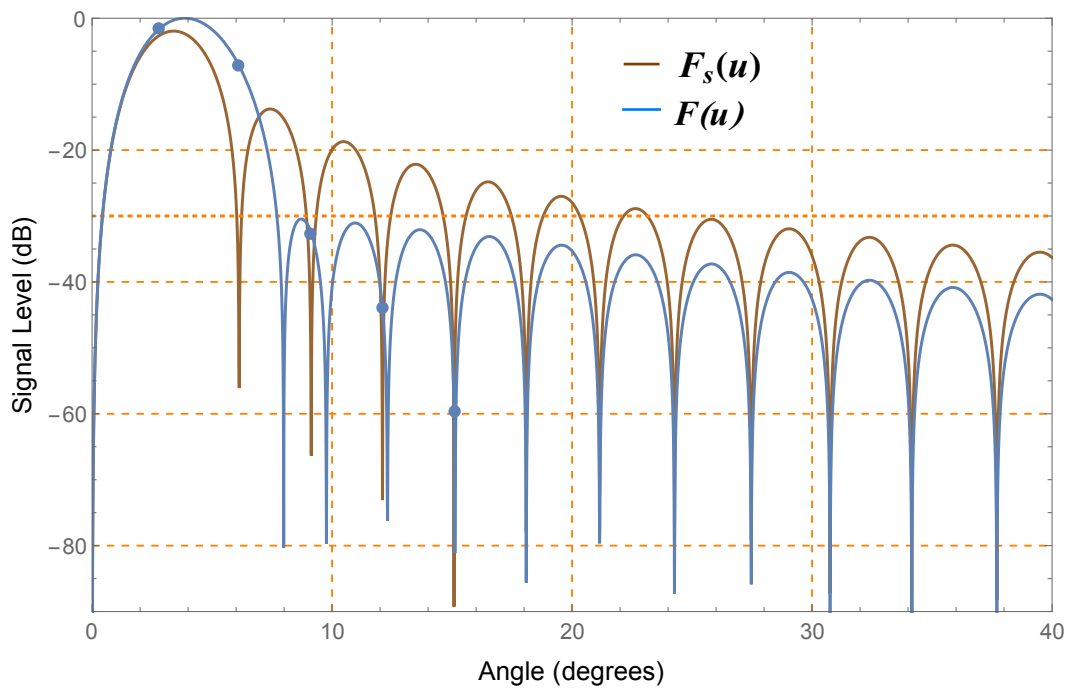
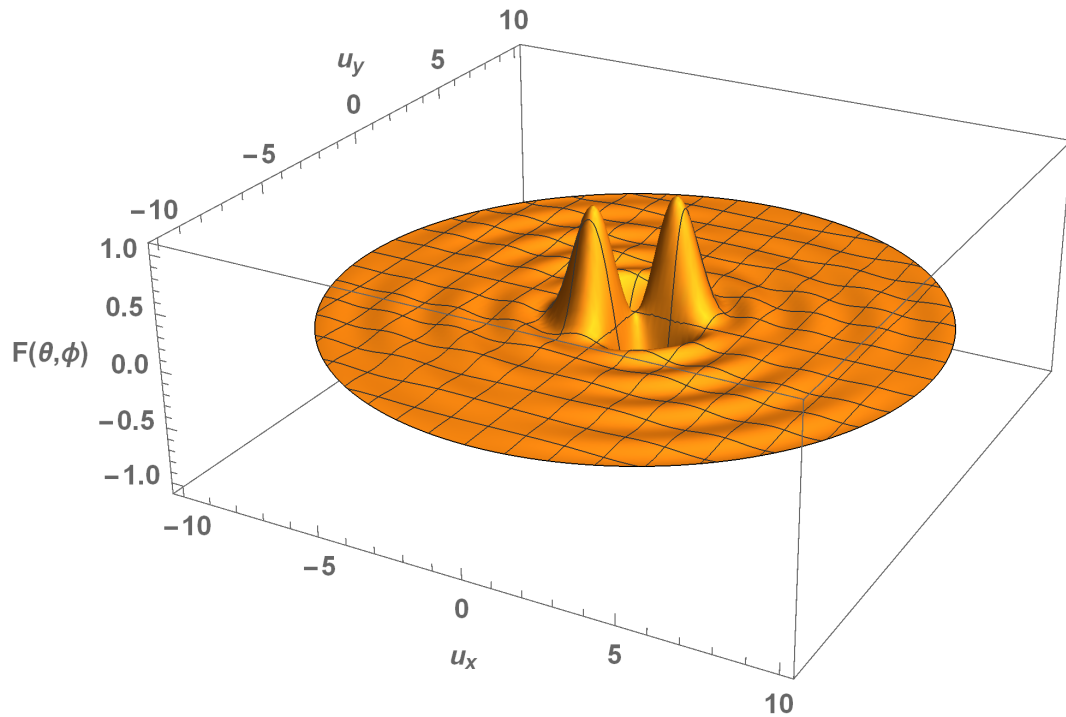
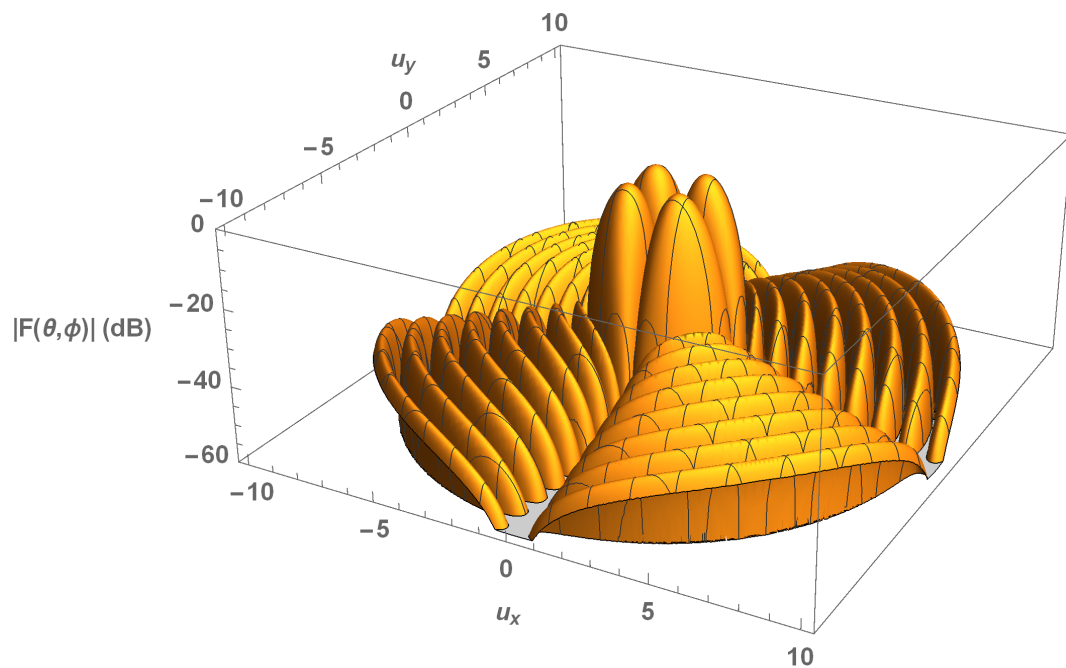


Figure 17: Comparison of delta-delta and starting function radiation patterns in the plane $\phi = 45^\circ$ for a 10 wavelengths radius antenna with -30 dB sidelobes



(i) Linear Scale



(ii) decibel Scale

Figure 18: Perspective view of delta-delta radiation pattern for 10 wavelengths radius antenna with -30 dB sidelobes, $M = 5$

We now use exactly the same arguments in finding an expression for the radiated field in terms of the aperture expansion as used in the Bayliss design, and find that

$$\begin{aligned} F(\mu_{2,l}) &= \frac{4}{\pi^2} B_{2,l} \pi \mu_{2,l} J_2(\pi \mu_{2,l}) \frac{J_2'(\pi u)}{\mu_{2,l}^2 - u^2} \Big|_{u \rightarrow \mu_{2,l}} \\ &= 2 B_{2,l} J_2(\pi \mu_{2,l})^2 \left\{ 1 - \frac{4}{\pi^2 \mu_{2,l}^2} \right\} \end{aligned} \quad (78)$$

It follows that

$$B_{2,l} = \frac{C_2}{4} \frac{\pi^2 \mu_{2,l}^2}{J_2(\pi \mu_{2,l})} \frac{\prod_{m=1}^{M-1} 1 - (\mu_{2,l}/\sigma u_m)^2}{\prod_{\substack{m=1 \\ m \neq l}}^M 1 - (\mu_{2,l}/\mu_{2,m})^2}, \quad l = 1, \dots, M-1 \quad (79)$$

There is a zero of $J_2'(\pi \mu)$ at the origin, similar to the zero in the Taylor design, but in this case, because $J_2(0)$ is equal to zero (figure 15) in equation 17, this does not contribute to the aperture field.

Thus we find

$$E_a(p, \psi) = \frac{C_2}{4} \sin 2\psi \sum_{l=0}^{M-1} \pi^2 \mu_{2,l}^2 \frac{J_2(p \mu_{2,l})}{J_2(\pi \mu_{2,l})} \frac{\prod_{m=1}^{M-1} 1 - (\mu_{2,l}/\sigma u_m)^2}{\prod_{\substack{m=1 \\ m \neq l}}^M 1 - (\mu_{2,l}/\mu_{2,m})^2} \quad (80)$$

Figure 19 shows the aperture distribution functions in the plane $\psi = 45^\circ$ to produce the radiation patterns of the two previous examples. There seems little difference between the aperture fields in increasing the value of M . For the case $M = 5$, the maximum aperture field is 3.4 at $\rho = 5.6$ wavelengths, and at the edge is 1.53. For the second example, $M = 8$, the respective figures are 3.59 at 5.62 wavelengths, and 1.50 at the edge. Figure 20 gives a perspective view of the aperture field of the $M = 5$ example above, emphasising the modulation of the radial distribution by the term $\sin 2\psi$ in the field expansion.

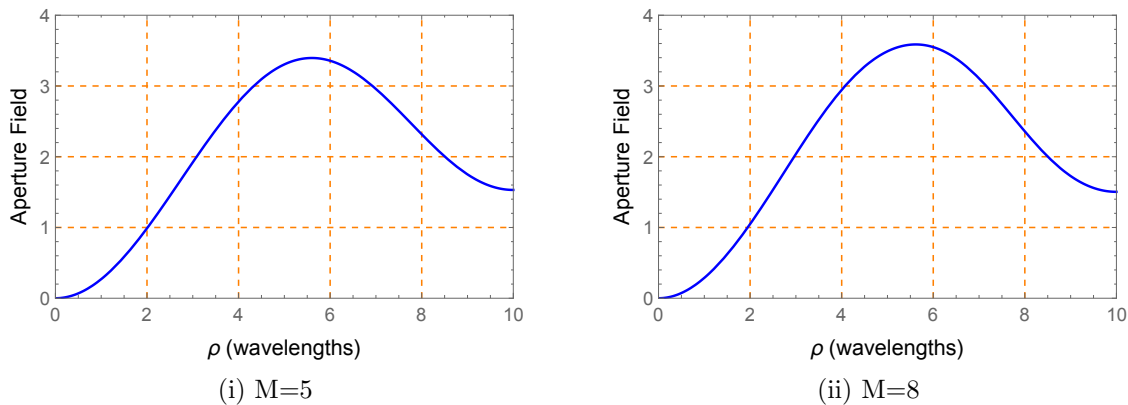


Figure 19: Delta delta aperture distribution in the plane $\psi = 45^\circ$ for 10 wavelengths radius antenna with -30 dB sidelobes

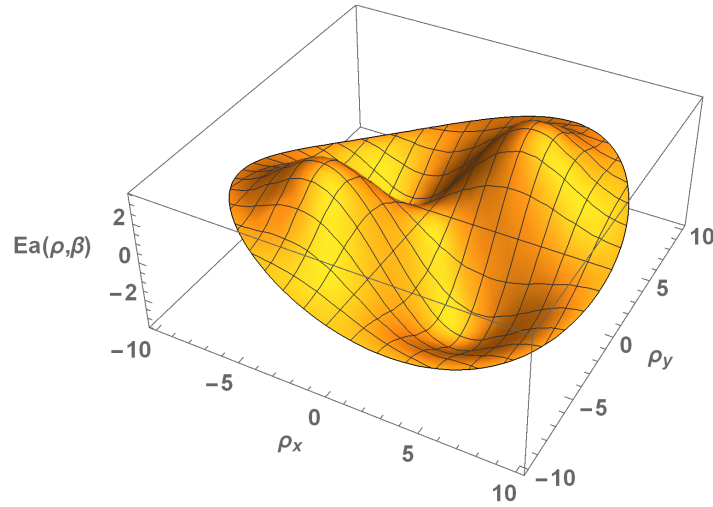


Figure 20: Perspective view of delta-delta aperture field for the radiation pattern of Figure 19(i)

4. Directivity, Aperture Efficiency, and Noise Properties of Aperture Distributions

In section 2 we began our study with the expression

$$E(r, \theta, \phi) = \frac{jkAe^{-jkr}}{2\pi r} \frac{1 + \cos \theta}{2} F(\theta, \phi) \quad (81)$$

for the electric field strength, E , at the point (r, θ, ϕ) in the far field of an aperture. We now wish to investigate the effect the aperture field distribution has on antenna gain, effective area, and signal-to-noise ratio, which are of more direct interest in the studies of radar system performance that we wish to undertake. Introducing

$$\begin{aligned} K &= \frac{jkA}{2\pi} \\ &= j \frac{A}{\lambda} \end{aligned} \quad (82)$$

and ignoring the obliquity factor, $(1 + \cos \theta)/2$, as we are only interested in gains in directions close to boresight, the power flux density, \mathcal{P} , assuming plane wave conditions at (r, θ, ϕ) , is

$$\mathcal{P}(r, \theta, \phi) = \frac{1}{2Z_0 r^2} |K|^2 |F(\theta, \phi)|^2 \quad (83)$$

Since $F(\theta, \phi)$ is normalised to 1 at its peak value in each of the aperture distributions considered, on substituting for $|K|$ from equation 82, the peak power flux density is

$$\mathcal{P}_{\text{peak}} = \frac{A^2}{2Z_0 \lambda^2 r^2} \quad (84)$$

The total radiated power, P_t , is determined by integrating the power flux density across the

aperture, on the assumption that the field near the aperture is a locally plane wave. Thus

$$\begin{aligned} P_t &= \frac{1}{2 Z_0} \int_A E_a^2(\rho, \psi) \rho d\rho d\psi \\ &= \frac{a^2}{2 \pi^2 Z_0} \int_0^{2\pi} \int_0^\pi E_a^2(p, \psi) p dp d\psi \end{aligned} \quad (85)$$

where $p = \pi\rho/a$. The expansion of the aperture field from section 2 is

$$E_a(p, \psi) = \sum_n \sum_{l=0}^{\infty} B_{n,l} e^{jn\psi} J_n(\mu_{n,l} p) \quad (86)$$

with n taking the values $0, \pm 1$, and ± 2 , for the Taylor, Bayliss and delta-delta designs, respectively. In view of the choices of the $B_{n,l}$ in the pattern designs, the exponential terms for each expansion can be combined to provide,

$$E_a(p, \psi) = b_n \sum_{l=0}^{M-1} B_{n,l} \cos(n\psi) J_n(\mu_{n,l} p) \quad (87)$$

where $b_n = 1$ for the Taylor design, and $b_n = 2$ for the Bayliss and delta-delta designs. It does not matter whether we use the cosine or the sine functions for the calculation of the radiated power of the Bayliss and delta-delta designs, but choosing the cosine gives a convenient way of considering all three aperture designs in a unified fashion. Substituting for E_a in equation 85 we find that

$$P_t = \frac{a^2 b_n^2}{2\pi^2 Z_0} \int_0^{2\pi} \int_0^\pi \cos^2(n\psi) p \left(\sum_{l=0}^{M-1} B_{n,l} J_n(\mu_{n,l} p) \right)^2 dp d\psi \quad (88)$$

The integral over ψ is simple to evaluate; it has the value 2π for $n = 0$ and the value π for all other n . However, the integral over p is somewhat complicated. Expanding out the square of the sum produces square terms of the form $J_n(\mu_{n,l} p)^2$ and cross product terms of the form $J_n(\mu_{n,l} p) J_n(\mu_{n,m} p)$. Dealing with the cross products first, from the recurrence relationships of the Bessel functions [1], we find that

$$\begin{aligned} J_{n-1}(\pi \mu_{n,l}) &= J_n'(\pi \mu_{n,l}) + \frac{n}{\pi \mu} J_n(\pi \mu_{n,l}) \\ &= \frac{n}{\pi \mu_{n,l}} J_n(\pi \mu_{n,l}) \end{aligned} \quad (89)$$

since the $\mu_{n,l}$ are the zeros of $J_n'(\pi \mu_{n,l})$. Thus if we expand the integral of the cross product terms, as determined using *Mathematica* [18] for the first line and then substitute for the $J_{n-1}(\pi \mu_{n,l})$ from equation 89, it follows that

$$\begin{aligned} \int_0^\pi p J_n(\mu_{n,l} p) J_n(\mu_{n,m} p) dp &= \frac{\pi \mu_{n,l} J_{n-1}(\pi \mu_{n,l}) J_n(\pi \mu_{n,m}) - \pi \mu_{n,m} J_{n-1}(\pi \mu_{n,m}) J_n(\pi \mu_{n,l})}{\mu_{n,m}^2 - \mu_{n,l}^2} \\ &= \frac{n J_n(\pi \mu_{n,l}) J_n(\pi \mu_{n,m}) - n J_n(\pi \mu_{n,m}) J_n(\pi \mu_{n,l})}{\mu_{n,m}^2 - \mu_{n,l}^2} \\ &= 0 \end{aligned} \quad (90)$$

indicating that the cross product terms do not contribute to the integral. Again using *Mathematica* [18] to evaluate the integral of the square terms, and substituting for $J_{n-1}(\pi\mu)$ from equation 89

$$\begin{aligned} \int_0^\pi p J_n(\mu_{n,l} p)^2 dp &= \frac{\pi^2}{2} J_{n-1}(\pi\mu_{n,l})^2 - \frac{\pi n}{\mu_{n,l}} J_{n-1}(\pi\mu_{n,l}) J_n(\pi\mu_{n,l}) + \frac{\pi^2}{2} J_n(\pi\mu_{n,l})^2 \\ &= \frac{\pi^2}{2} J_n(\pi\mu_{n,l})^2 \left(1 - \frac{n^2}{\pi^2 \mu_{n,l}^2}\right) \end{aligned} \quad (91)$$

Thus the expression for the radiated power of the aperture becomes

$$P_t = \frac{b_n A}{2 Z_0} \sum_{l=0}^{M-1} B_{n,l}^2 J_n(\pi\mu_{n,l})^2 \left(1 - \frac{n^2}{\pi^2 \mu_{n,l}^2}\right) \quad (92)$$

It follows that the directivity of the antennas is

$$D = 4\pi \frac{A}{\lambda^2} \left[b_n \sum_{l=0}^{M-1} B_{n,l}^2 J_n(\pi\mu_{n,l})^2 \left(1 - \frac{n^2}{\pi^2 \mu_{n,l}^2}\right) \right]^{-1} \quad (93)$$

and that the effective aperture is

$$A_{\text{eff}} = A \left[b_n \sum_{l=0}^{M-1} B_{n,l}^2 J_n(\pi\mu_{n,l})^2 \left(1 - \frac{n^2}{\pi^2 \mu_{n,l}^2}\right) \right]^{-1} \quad (94)$$

The specific results for the three antenna designs that are the subject of this report are

Taylor

$$A_{\text{eff}} = A \left[1 + \sum_{l=1}^{M-1} B_{0,l}^2 J_0(\pi\mu_{0,l})^2 \right]^{-1} \quad (95)$$

Bayliss

$$A_{\text{eff}} = A \left[2 \sum_{l=1}^{M-1} B_{1,l}^2 J_1(\pi\mu_{1,l})^2 \left(1 - \frac{1}{\pi^2 \mu_{1,l}^2}\right) \right]^{-1} \quad (96)$$

and

Delta-delta

$$A_{\text{eff}} = A \left[2 \sum_{l=1}^{M-1} B_{2,l}^2 J_2(\pi\mu_{2,l})^2 \left(1 - \frac{4}{\pi^2 \mu_{2,l}^2}\right) \right]^{-1} \quad (97)$$

with the respective directivities being these expressions multiplied by $4\pi/\lambda^2$.

Table 2 provides a comparison of the antenna parameters for the three designs of a 10 wavelength radius antenna with -35 dB design sidelobe level for the Taylor, and -30 dB sidelobe levels for the Bayliss and delta-delta designs. In each case $M = 5$. The effective area is in units of square wavelengths, whereas the aperture field strengths are ratios to the uniform

aperture case and are dimensionless. The aperture design and aperture efficiency are independent of the radius of the antenna for any fixed values of both the sidelobe level and M , which is evident in the mathematical development in Section 2. Both antenna directivity and effective area are proportional to the physical area, and thus the figures for the table parameters can be scaled for other antenna diameters. Note though that M has to be sufficiently large to ensure that the subsequent unshifted nulls do not have sidelobes in excess of the design sidelobe level; thus significantly larger apertures may require an increase in M , and that will result in changes from the parameters presented in the table.

Table 2: Comparison of parameters of the antenna designs for a 10 wavelength radius antenna

Parameter	Uniform	Taylor	Bayliss	Delta-Delta
Directivity (dB)	35.96	34.87	32.55	31.06
Beam broadening σ	1.0	1.105	1.090	1.067
Effective area	314.2	244.4	143.2	101.5
Aperture efficiency	1.0	0.778	0.456	0.323
Peak aperture field	1.0	2.258	3.006	3.395
Edge aperture field	1.0	0.450	1.028	1.531

The figures for directivity show that a loss of about 1.1 dB is incurred with Taylor weighting, about 3.4 dB for Bayliss weighting, and 4.9 dB for delta delta, compared with the uniform aperture. However, to maintain the same transmitted field strength for the three designs⁹ the maximum aperture field strength has to be 2.258, 3.006 and 3.395 times, respectively, that for a uniformly illuminated aperture. For an aperture weighting achieved with an appropriately shaped feed horn illuminating a parabolic dish, and fed by a single power source, or for a passive electronically scanned phased array with a lossless corporate feed to the antenna elements, again fed by a single power source, these figures would be of no concern. The directivities of the table are what would be observed in practice. However, for an active electronically scanned phased array, the maximum transmit power of each T/R module is fixed. Since the aperture distribution in this case is achieved by tapering the output power level of the T/R modules, the total transmit power of the array is significantly reduced, and with it, the radiated field strength. The peak aperture fields in Table 2 imply a loss of 7.07 dB in peak transmitted field strength for the Taylor weighting¹⁰, 9.56 dB for the Bayliss weighting and 10.62 dB for the delta-delta weighting, compared with the uniform array. Clearly the use of antenna directivity for field strength and received power calculations of active electronically scanned phased array radar systems needs careful scrutiny.

In comparing the signal levels received by the arrays, use will be made of the reciprocity theorem for antennas; this theorem appears in a variety of forms, [11]; we shall use the one which states that “*The receiving pattern of any antenna constructed of linear isotropic matter is identical to its transmitting pattern*”. Consider now an active aperture populated by a large

⁹Because the theory of the designs has been based on the radiated fields arising from prescribed aperture distributions, we continue the discussion here as if radar systems transmit all these beam shapes. Most radar systems transmit a uniform aperture distribution and receive the sum signal with a low sidelobe beam. We are not aware of any systems that transmit the difference or double difference beams for surveillance purposes.

¹⁰An additional loss of a few dB is incurred with the Taylor weighted transmission because the T/R modules must be operated in their linear region, and not in saturation. The total loss in transmitted field strength makes it highly desirable to transmit with a uniform aperture field, and use low sidelobes on reception to control the sidelobe clutter levels.

number of active antenna elements, N in all, with a number of passively loaded elements surrounding the aperture to ensure that the active elements have a uniform impedance environment. On reception of a reflected signal from a remote target, the field incident on the array will be essentially a plane wave, of power flux density \mathcal{P}_i , and the received power by each antenna element will be $p_i = A_e \mathcal{P}_i$, where A_e is the effective area of the element in the array. In the case of the uniform array, these signal levels are added in phase giving a received power¹¹

$$\begin{aligned} P_r &= \mathcal{P}_i A_e N^2 \\ &= \mathcal{P}_i A_{\text{eff}} N \end{aligned} \quad (98)$$

where A_{eff} is the effective area of the whole array. For the other array designs, though, the outputs from the elements of the array are tapered to provide the desired radiation pattern, and this will result in a loss of received power. Appealing to reciprocity, this loss is the same as the loss discussed in the preceding paragraph, i.e., the received powers of the Taylor, Bayliss and delta-delta designs will be 7.07, 9.56, and 10.62 dB less than for the uniform aperture.

The preceding figures seem alarming, but what is missing from the discussion of the antenna parameters is a calculation of the noise level at the output of the array manifold after beamforming. We will assume that each of the antenna elements in the array has the same noise temperature T . Similarly, there is an impedance loss L within each antenna element and in the transmission line and circulators between the antenna and the input to the transmit/receive module, and these receiver modules have a noise figure \mathcal{F} . The outputs of these modules are summed in a passive lossless manifold, the inputs of which are weighted to approximate the aperture distributions of the uniform, Taylor, Bayliss and delta-delta designs. The noise power n_o , at the output of each transmit/receive module is

$$n_o = \frac{kTBg}{L} + \frac{kT_0B(L-1)}{L} + kT_0B(\mathcal{F}-1) \quad (99)$$

and thus if the loss factor is L_k for the k th T/R module, then the total noise power at the output of the manifold after summing over the N elements is

$$\begin{aligned} n &= \sum_{i=1}^N n_o L(\psi_i, p_i) \\ &= N n_o \times \text{average of aperture power distribution function} \end{aligned} \quad (100)$$

where by $L(\psi_i, p_i)$ we indicate the manifold coupling factor for the i^{th} antenna element whose coordinates in the array are (ψ_i, p_i) . For the uniform aperture this simplifies to $N n_o$, but for the other distribution functions, for large N , this approaches the normalised power distribution of the aperture averaged over the area of the aperture. We now introduce a constant C , whose value is the inverse of the peak aperture field of the respective designs, to set the maximum value of the $L(\psi_i, p_i)$ to 1; in the case of the uniform distribution $C = 1$. The average of the aperture power distribution is obtained from equation 92 by normalising it by the factor C^2 ,

¹¹In implementing the summing with a hybrid-T junction or a similar device, the signal power in each input port will combine to increase the output by 3 dB, whereas the noise output will stay the same as in each input port. As we are interested only in the signal-to-noise ratio, we have not included this normalisation in our expressions.

dividing by A , and discarding the factor $2 Z_0$ which pertains to the E field power calculations. Thus the total noise power at the output of the manifold is

$$n = N n_o C^2 b_n \sum_{l=0}^{M-1} B_{n,l} J_n(\pi \mu_{n,l})^2 \left(1 - \frac{n^2}{\pi^2 \mu_{n,l}^2}\right) \quad (101)$$

which will enable a comparison of the output noise levels of the different antenna designs.

Since the signal power is also scaled by C^2 , this parameter disappears and we find that the output signal-to-noise ratio is proportional to

$$\frac{s}{n} \propto \left[b_n \sum_{l=0}^{M-1} B_{n,l} J_n(\pi \mu_{n,l})^2 \left(1 - \frac{n^2}{\pi^2 \mu_{n,l}^2}\right) \right]^{-1} \quad (102)$$

which is identified as the aperture efficiency. Thus despite the large loss in received signal strength, the overall loss in signal-to-noise ratio compared with the uniform array is modest, 1.09 dB for the Taylor, 3.41 dB for the Bayliss, and 4.91 dB for the delta-delta designs discussed in this report.

The final parameter of interest is the monopulse ratio, the ratio of the Bayliss signal amplitude to the Taylor amplitude in the absence of noise, and in particular the slope at the curve at the origin. In the limit of small u , forming the ratio of equation 56 to equation 33, and taking account of the relative voltages of the Taylor and Bayliss signals, we have

$$\mathcal{R} = -\frac{C_1 R \pi^2 u^2 J_1'(\pi u)}{2 J_0'(\pi u)} \quad (103)$$

where R is the ratio of the respective aperture field terms from Table 2. The product terms in the respective equations of the Taylor and Bayliss expansions are all of second and higher orders and have been discarded. At the origin $J_1'(\pi u)$ is equal to 0.5 (Figure 2), whereas $J_0'(\pi u)/\pi u$ has the value -0.5 (Figure 3), and thus for small u ,

$$\mathcal{R} = 0.5 \pi u C_1 R \quad (104)$$

With *Mathematica*, it is possible to find much better approximations to the monopulse ratio, by expanding the ratio of equation 56 to equation 33 in powers of u using the function `Series`. Including the scaling factors, the ratio to 6th order is

$$\mathcal{R} = C_1 R (1.5708 u + 0.385478 u^3 + 0.119627 u^5 + O[u]^7) \quad (105)$$

Figure 21 compares the monopulse ratio determined directly from equations 33 and 56 with appropriate scaling factors (blue), with progressively, the sum of the terms of equation 105, i.e. the first order (brown), the third order (green), and fifth order approximations (red), for a 10 wavelengths radius antenna. By chance, the slope at the first order approximation is almost precisely 0.5 per degree, and within about 1 degree, this gives a quite accurate estimate of the target angular position. For the Taylor pattern the half-power beamwidth for a 10 wavelength radius antenna is 3.56 degrees, and thus the monopulse measurement requires no more than the simple slope term for target positioning within the central 56% of this region. At greater angles a more precise inverse of the ratio is required. The third order approximation gives

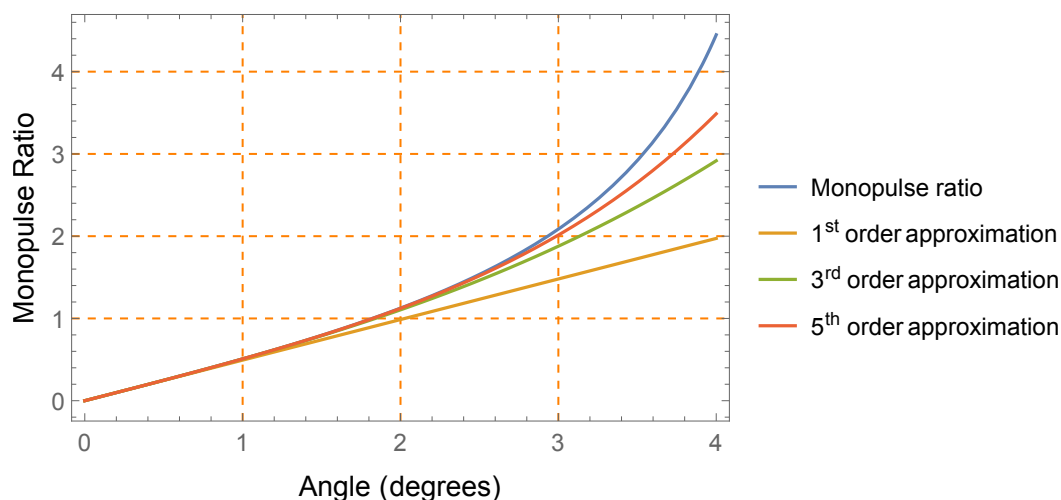


Figure 21: Comparison of monopulse ratio with first, third, and fifth order approximations to the ratio for a 10 wavelengths radius aperture

excellent results out to about 2 degrees, in excess of the beamwidth of the sum antenna. The fifth order result is a slight improvement on the third and has reasonable accuracy to about 2.8 degrees. Since in a radar, the receive fields provide an estimate of the monopulse ratio, there is a requirement to find the inverse of this ratio to determine the angular position of the target. For the first order approximation, the inverse is simple to determine. However for the third order approximation, it is much more complex as it involves solving a cubic equation. *Mathematica* can be used to provide the solution. For the fifth order approximation, an iterative procedure is required to determine the target position.

5. Conclusions

This report provides a unified approach to the design of the sum, difference, and delta-delta antenna radiation patterns used in modern-pulse Doppler radar systems. Examples of each design are presented for a 10 wavelengths radius aperture for both 5 and 8 zero position changes. Both radiation patterns and aperture distributions of these cases are provided. It is shown how associated antenna parameters, the gain, effective aperture, and aperture efficiency can be calculated, and advises care in the use of these parameters in calculating radar system performance. The Appendix provides a brief discussion of the approach in implementing this work in *Mathematica*.

References

- [1] M.Abramowitz and I.A.Stegun, "Handbook of Mathematical Functions", Dover Publications, New York, 1965
- [2] C.A.Balanis, "Antenna Theory, Analysis and Design, Harper & Row, New York, 1982
- [3] E.T.Bayliss, "Design of Monopulse Antenna Difference Patterns with Low Sidelobes", Bell System Technical Journal, Vol 47, May-June 1968, pp 623-650
- [4] G.F.Carrier, M.Krook, and C.E.Pearson, "functions of a complex variable", McGraw Hill, New York, 1966
- [5] D.E.Chesley, "Design of a Low Sidelobe Double Difference Beam for a Circular Aperture", IEEE Transactions on Antennas and Propagation, Vol AP-40, No 10, October 1992, pp 1187-1191
- [6] R.S.Elliott, ' Design of Circular Apertures for Narrow Beamwidth and Asymmetric Low Sidelobes", IEEE Transactions on Antennas and Propagation, Vol AP-23, No 4, July 1975, pp 523-527
- [7] R.S.Elliott, "Antenna Theory and Design", IEEE Press Series on Electromagnetic Wave Theory, 2003
- [8] R.S.Elliott, "Design of Line Source Antennas for Difference Patterns with Sidelobes of Individually Arbitrary Heights", IEEE Transactions on Antennas and Propagation, Vol AP-24, No 3, May 1976, pp 310-316
- [9] I.S.Gradshcheyn and I.M.Ryzhik, "Tables of Integrals, Series, and Products", Academic Press, New York, 3rd Edition, 1966
- [10] R.C.Hansen, "Tables of Taylor Distributions for Circular Aperture Antennas", IRE Transactions on Antennas and Propagation, Vol AP-3, pp 23-26, January 1960
- [11] R.F.Harrington, "Time Harmonic Electromagnetic Fields", McGraw Hill, New York, 1961
- [12] R.R.Kinsey, "Monopulse Difference Slope and Gain Standards", IRE Transactions on Antennas and Propagation, Vol AP-5, pp 343-4, May 1962
- [13] J.J.Lee, "G/T and Noise Figure of Active Array Antennas", IEEE Transactions on Antennas and Propagation, Vol AP-41, No 2, February 1983, pp 241-244
- [14] P.Z.Peebles, Jr. "Radar Principles", Wiley Interscience, New York, 1998
- [15] J.Ruze, "Circular Aperture Synthesis", IEEE Transactions on Antennas and Propagation, Vol AP-12, November 1964, pp 691-694

- [16] T.T.Taylor, "Design of Circular Apertures for Narrow Beamwidth and Low Sidelobes", IRE Transactions on Antennas and Propagation, Vol AP-3, No 1, January 1960, pp 17-22
- [17] J.L.Whitrow, "Scanning and Beam Placement in Pulse Doppler Radar Systems", DST Technical Report, (in publication)
- [18] S. Wolfram, *Wolfram Mathematica*, v11.1.0
- [19] *Mathematica* notebook `Taylor.nb` Objective ref. AV15216884
- [20] *Mathematica* notebook `Bayliss.nb` Objective ref. AV15216882
- [21] *Mathematica* notebook `DeltaDelta.nb` Objective ref. AV15216883
- [22] *Mathematica* language file `PhasedArray.wl` Objective ref. AV15216886

UNCLASSIFIED

DST-Group-TR-3487

This page is intentionally blank

UNCLASSIFIED

Appendix A. Implementation of the Algorithms in Mathematica

The algorithms discussed in this report have been implemented with the use of *Mathematica* for inclusion in a radar performance modelling package. There are separate notebooks¹² for Taylor, Bayliss and delta-delta calculations that have been used in the development of the software and for the preparation of figures in this report. Many of the integration expressions used in the report are also confirmed in the notebooks. Separate to these but containing the antenna pattern algorithms from the notebooks is a `.wl` file (Wolfram language file, previously a `.m` file) for use with our radar models. In the software an additional letter `t`, `b`, or `d`, is added to the original parameters from the mathematical expressions to distinguish whether the parameters pertain to the Taylor, Bayliss or delta-delta designs, as in μt , μb , and μd ¹³.

A.1. The Setup Procedure

Given that in any simulation study, the parameters of the antenna will be fixed for the duration of the simulation, each antenna model is initiated with a set-up procedure, `PhasedArraySetup`, to generate the positions of the zeros of the model function and the starting function, and store them in a region accessed by the antenna gain calculation.

The setup for the Taylor distribution is the simplest. Given the design parameters, sidelobe level, `SLL` and `M`¹⁴, the steps in the procedure are

1. calculate the value of `A` to provide the correct sidelobe level for the model function
2. find the first `M` positive zeros of $J_0'(\pi\mu)$ and store them in `μt`
3. find the first `M` zeros of the model function and store them in `unt`
4. calculate the beam broadening factor σ
5. multiply the `unt` by σ .
6. delete the last member of both `unt` and `μt` , and store these lists where the antenna field algorithms can access them.
7. calculate the aperture field strength, and determine the maximum value, `Emaxt`
8. calculate the effective aperture `EffApt`
9. store `Emaxt` and `EffApt` for subsequent use by the antenna field algorithms

¹²Notebooks are a Wolfram construct for interfacing with the *Mathematica* kernel, and maintaining collections of calculations.

¹³*Mathematica* allows the use of Greek letters as parameters in code

¹⁴In the *Mathematica* software used to implement the algorithms designed in this report, summation and/or multiplication over lists does not require an index such as the l and m used in the text of this report

The Bayliss setup is more complex. The Bayliss software only allows sidelobe levels to be chosen in intervals of 5 dB between -15 dB and -40 dB. The steps in the setup are

1. select the parameters **A**, and $\xi_1, \xi_2, \xi_3, \xi_4$ from tables of parameters for the nearest 5 dB sidelobe level to the requested sidelobe level
2. populate $\mu\mathbf{b}$ with the first $M+1$ zeros of $J_1'(\pi\mu)$.
3. calculate the zeros \mathbf{unb} of the model function, note that this is more complex than the Taylor calculations as the first four zeros are replaced by the ξ_1, \dots, ξ_4 .
4. calculate the value of the beam broadening factor σ
5. multiply the \mathbf{unb} by σ
6. `BaylissAntGain` is called to determine the location and value of the maximum of the Bayliss radiation pattern,
7. the scale factor \mathbf{Gb} , which previously has the value 1.0, is calculated to be used to scale all subsequent calls to `BaylissAntGain` to a maximum value of 1.0 (0 dB)
8. delete the last member of \mathbf{unb} and $\mu\mathbf{b}$, and return these and \mathbf{Gb} to storage for future use.
9. calculate the aperture field strength, and determine the maximum value \mathbf{Emaxb}
10. calculate the effective aperture \mathbf{EffApb}
11. store \mathbf{Emaxb} and \mathbf{EffApb} for subsequent use by the antenna field algorithms

The delta-delta setup is similar, but as the model function is expressed as the difference between two Taylor type model functions, the zeros \mathbf{und} of this function have to be calculated using the *Mathematica* function `FindRoot`. The steps in the procedure are

1. calculate the parameters $\mathbf{A1}$ and $\mathbf{A2}$ according to guidelines by Chesley for these parameters, and the parameter \mathbf{K} obtained from the ratio
2. calculate the position of the zeros of the $\mathbf{A2}$ aperture function and store them in \mathbf{rn}
3. calculate the precise positions of the zeros \mathbf{und} of the model function using `FindRoot` with the \mathbf{rn} as starting points for this calculation.
4. determine the positions of the first $M+1$ zeros of the $J_2'(\pi\mu)$ using `FindRoot`, starting with values of the form $m + 0.25$, and store them in $\mu\mathbf{d}$.
5. calculate the scale factor σ and multiply \mathbf{und} by this factor.

6. determine the maximum value of `DeltaAntGain` using `Findmaximum` and store this in `Gd` to scale all subsequent calls to `DeltaAntGain` to have a peak value of 1.0 (0 dB).
7. delete the last member of `μd` , and of `und`, and store these lists and `Gd` for future use in antenna field calculations.
8. calculate the aperture field strength, and determine the maximum value `Emaxd`
9. calculate the effective aperture `EffApd`
10. store `Emaxd` and `EffApd` for subsequent use by the antenna field algorithms

A.2. Calculation of the Antenna Fields

Much of the algorithms for the different field patterns are common, so `PhasedArrayField` is designed to calculate the transmitted and received fields of the uniform, Taylor and Bayliss patterns and return them as a four element list, rather than separately call three functions. The first action is to calculate the value of u . In this report it is simply $2a \sin \theta$, where θ is the angle between the normal to the array and the field point. In the software, it is a function of both the scan angle and the direction of the field point, and is also modified by the orientation of the array. These matters are discussed in a separate report [17], so for now we will leave it as described above. The steps in the software procedure are

1. calculate the value of u
2. calculate the obliquity factor $(1.0 + \cos[\theta]) / 2.0$
3. if $u=0$, return $\{1.0, 1.0, 0.0, 0.0\}$ for the four fields
4. otherwise calculate expansions for the space factors of uniform, Taylor and Bayliss azimuth and elevation fields; these are basically single line expressions for the fields described in equations 33, 56 and 73
5. return the product of the obliquity factor and the four space factors.

Mathematica notebooks containing the development of the algorithms discussed in this report are included in Objective along with this report. These notebooks give details of various functions that were investigated in the development process, and the tests that were carried out on the algorithms to verify correct functioning. The notebooks are `Taylor.nb` [19], `Bayliss.nb` [20], and `DeltaDelta.nb` [21]. Also included is a *Mathematica* language file `PhasedArray.wl` giving the final coded form of the software for calculating uniform, Taylor and Bayliss radiation patterns. For the present, the delta-delta algorithm is not included in this software as it is not required for the current studies. Inclusion is quite straightforward, along the lines of the Bayliss model, but it returns only one field value.

UNCLASSIFIED

DEFENCE SCIENCE AND TECHNOLOGY GROUP DOCUMENT CONTROL DATA		1. DLM/CAVEAT (OF DOCUMENT)	
2. TITLE The Radiation Patterns of Circular Apertures		3. SECURITY CLASSIFICATION (FOR UNCLASSIFIED LIMITED RELEASE USE (L) NEXT TO DOCUMENT CLASSIFICATION) Document (U) Title (U) Abstract (U)	
4. AUTHOR Dr J L Whitrow		5. CORPORATE AUTHOR Defence Science and Technology Group PO Box 1500 Edinburgh, South Australia 5111, Australia	
6a. DST GROUP NUMBER DST-Group-TR-3487	6b. AR NUMBER 017-177	6c. TYPE OF REPORT Technical Report	7. DOCUMENT DATE May, 2018
8. OBJECTIVE ID U920600	9. TASK NUMBER AIR 17/518	10. TASK SPONSOR Head JSF	
11. MSTC Surveillance & Radar Systems		12. STC Signatures & Phenomenology	
13. DOWNGRADING/DELIMITING INSTRUCTIONS http://dspace.dsto.defence.gov.au/dspace/		14. RELEASE AUTHORITY Chief, National Security and ISR Division	
15. SECONDARY RELEASE STATEMENT OF THIS DOCUMENT <i>Approved for Public Release</i>			
<small>OVERSEAS ENQUIRIES OUTSIDE STATED LIMITATIONS SHOULD BE REFERRED THROUGH DOCUMENT EXCHANGE, PO BOX 1500, EDINBURGH, SA 5111</small>			
16. DELIBERATE ANNOUNCEMENT No Limitations			
17. CITATION IN OTHER DOCUMENTS No Limitations			
18. RESEARCH LIBRARY THESAURUS circular antenna design, antenna gain, Taylor weighting, Bayliss weighting, delta-delta weighting			
19. ABSTRACT Taylor, Bayliss, and Chesley are names associated with the design of antennas for modern pulse Doppler radar systems. This report provides a unified approach to the design techniques that they used to achieve the specified beam shape and sidelobe levels that are key performance requirements for airborne pulse-Doppler signal processing. A number of ancillary factors on signal and noise levels in the use of these antenna designs are discussed.			

UNCLASSIFIED